Carnegie-Mellon University
PITTSBURGH, PENNSYLVANIA 15213

DEPARTMENT OF
MECHANICAL ENGINEERING

ISOFINEL: ISOPARAMETRIC FINITE ELEMENT CODE FOR ELASTIC ANALYSIS OF TWO-DIMENSIONAL BODIES

C. MARINO

Report SM-75-4

September 1975

The work described in this report was supported by the
National Aeronautics and Space Administration
NASA Research Grant NGR-39-087-053

ISOFINEL: ISOPARAMETRIC FINITE ELEMENT CODE FOR ELASTIC ANALYSIS OF TWO-DIMENSIONAL BODIES

C. Marino

Report SM-75-4 September 1975

The work described in this report was supported by the
National Aeronautics and Space Administration
NASA Research Grant NGR-39-087-053

Department of Mechanical Engineering
Carnegie Institute of Technology
Carnegie-Mellon University
Pittsburgh, Pennsylvania

ABSTRACT

This report presents a formulation for the development of a finite element program for the elastic analysis of two-dimensional bodies using the eight-node isoparametric quadrilateral. The program solves for both plane stress and plane strain problems.

A general development of the finite element formulation based on the isoparametric displacement functions is presented.

The program structure is given in the form of flow diagrams with descriptions of the numerical procedure used to obtain the element stiffness matrix, and the solution method employed to solve for nodal displacements.

Three numerical examples, a plate under uniaxial tension, a plate under pure shear, and a beam under pure bending are presented to illustrate the capability and limitations of the element implementation. The first problem is solved exactly by the element, as predicted by the form of its displacement functions. However, in the other two problems the accuracy of the solution is highly dependent upon the slenderness of the element, the number of elements in the map, and the numerical integration scheme used to build the element stiffness matrix.

The report ends with some recommendations concerning map generation, simplification of the input data, and extensions to solution of plasticity problems.

1. INTRODUCTION

The advantages of the isoparametric elements over the well-known constant strain triangle (CST) have been substantially demonstrated in the last few years. Based on the experience we have gained from the CST, development of a finite element program for isoparametric elements is highly desirable. As is described below, among the advantages of the isoparametric elements is their ability to be coupled with other isoparametric elements which may be convenient in many cases, and furthermore with other type of elements such as crack-tip elements currently being developed.

Among the numberless members of the isoparametric family, the four, eight, nine, and twelve node isoparametric quadrilaterals are the most popular for two-dimensional analysis, not only because the high order of their displacement functions but for their relative low cost in terms of computer time and input preparation. The efficiency of any particular element type used will depend on how well the shape functions are capable of representing the true displacement field. At the time we initiated this work, very little was known about the differences in accuracy between the eight and nine node parabolic elements. Primarily because of storage limitations, in particular in the transition to the elastoplastic version of the program (currently in process), we chose the eight node quadrilateral as the pattern element of the program.

The four node quadrilateral (Figure 1.1a) provides a linear displacement distribution. It has proved to be an efficient element since the construction of the stiffness matrix can be done in closed form, while

the higher order elements require the use of a numerical integration procedure. The nine and twelve node quadrilaterals (Figure 1.1c and 1.1d) produce parabolic and cubic displacement distributions within the element, respectively. The latter, although is very accurate in the handling of a large variety of problems, presents two major drawbacks. First, it requires a 4x4 Gauss integration procedure to build the stiffness matrix, which means both large storage and a high computer bill. Second, the bandwidth of the master stiffness matrix is usually larger than that of an eight node isoparametric for a comparable number of elements, which may provide storage problems, in addition to longer running time in the solving routine.

These reasons in addition to the results presented here and elsewhere [1-4]* prove the wise choice with the eight-node isoparametric.

---

*Numbers in brackets denote entries in the list of references following the text.

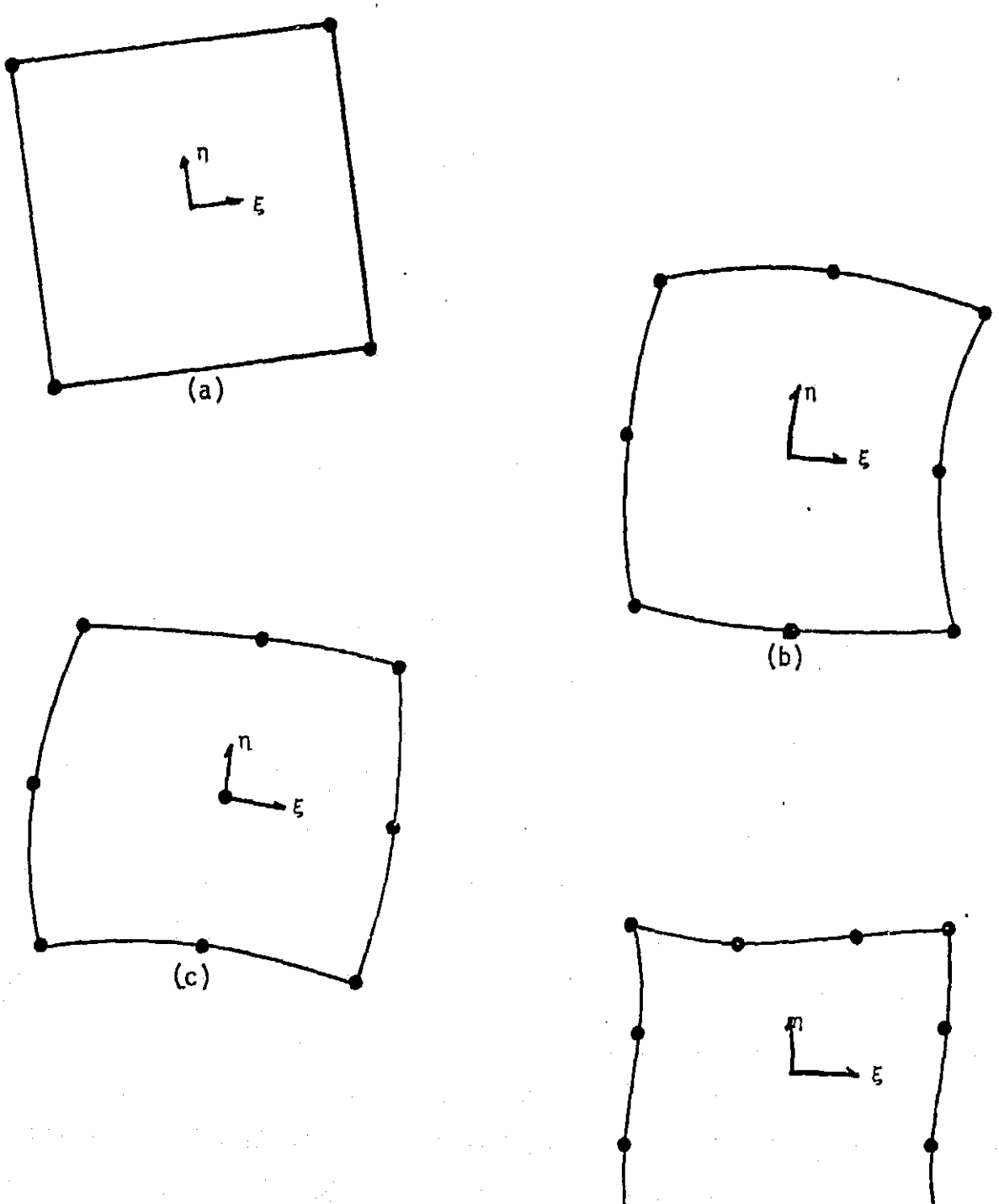

Figure 1.1 (a) Four-Node Isoparametric Quadrilateral
(b) Eight-Node Isoparametric Quadrilateral
(c) Nine-Node Isoparametric Quadrilateral
(d) Twelve-Node Isoparametric Quadrilateral

2. OVERVIEW

The basic step of any direct stiffness finite element analysis is the unique description of the unknown functions $\{\delta\}$, in this case they correspond to the displacement field within each element, in terms of n parameters $\{\delta_0\}$ given by

$$\{\delta\} = [N]\{\delta_0\} \tag{1}$$

where n = number of nodes for element,

$\{\delta_0\}$ = vector of nodal displacements, and

$[N]$ = matrix of shape functions evaluated at the point in the element where displacements are desired.

With displacements known at all points within the element, the strains at any point can be determined, resulting in a relationship of the form,

$$\{\varepsilon\} = [B]\{\delta\} \tag{2}$$

where the matrix $[B]$ is conformed by the partial derivatives of the shape functions given explicitly in Appendix A.

To satisfy equilibrium it is required that the forces acting on an element lumped as $\{f\}$ concentrated at the nodes must balance the stresses within the element. That is,

$$\int_A [B]^T\{\sigma\}dA - \{f\} = 0 \tag{3}$$

where A is the cross sectional area of the element where tractions are prescribed, and $\{\sigma\}$ is the stress vector.

For linear elasticity, the constitutive law between stresses and strains is

$$\{\sigma\} = [D]\,(\{\varepsilon\} - \{\varepsilon_0\}) + \{\sigma_0\} \tag{4}$$

where [D] is the elasticity matrix that differs slightly between the cases of plane stress and plane strain, and $\{\sigma_0\}$ and $\{\varepsilon_0\}$ are the initial stresses and strains, respectively. Substituting (2) and (4) into (3) we obtain for any element that

$$\{f\} = [k]\{\delta\} \tag{5}$$

with

$$[k] = \int_A [B]^T[D][B]dA \tag{6}$$

Once equilibrium is established at each node, and nodal displacement continuity is ensured, we may write for the complete structure a load-displacement relationship of the form,

$$\{F\} = [K]\,\{\delta\} \tag{7}$$

where [K] is an $\ell x \ell$ matrix, ℓ being the total number of degrees of freedom of the structure and is called the overall stiffness matrix.

To select an isoparametric element is to select a determined set of shape functions, which is not arbitrary. These are three minimum conditions which must be satisfied [1] in order to ensure convergence of the solution to the correct results:

(a) The shape functions must be continuous between elements;

(b) In the limit, as the element size is reduced to infinitesimal dimensions, the shape functions must be able to reproduce a constant strain condition throughout the element. This means that the unknown function must be able to take in the limit any linear form throughout the element.

(c) Rigid body motion is accomplished if every shape function satisfies the relation,

$$\sum_{i=1}^{n} N(\xi_i, \eta_i) = 1$$

2.1 Shape Functions for the 8-Node Quadrilateral

In the isoparametric formulation, the general relationship between the global cartesian coordinates (x,y) and the local curvilinear coordinates (ξ,η) is (Figure 2.1):

$$\begin{aligned} x &= N_1 x_1 + N_2 x_2 + \ldots = \{N\}^T \{x_n\} \\ y &= N_1 y_1 + N_2 y_2 + \ldots = \{N\}^T \{y_n\} \end{aligned} \tag{8}$$

where $N_i = f(\xi,\eta)$ are the isoparametric shape or displacement functions, and $\{x_n\}$, $\{y_n\}$ are the column vectors of the cartesian coordinates. For any values of ξ and η the x and y coordinates can be found once the functions N are known.

In finite element analysis of two-dimensional stress problems, it is necessary to define the variation of nodal displacement components u_i and v_i in terms of the nodal values of the displacement functions N_i. Thus we have:

$$\begin{aligned} u(\xi,\eta) &= N_1 u_1 + N_2 u_2 + \ldots + N_n u_n = \{N\}^T \{u_n\} \\ v(\xi,\eta) &= N_1 v_1 + N_2 v_2 + \ldots N_n v_n = \{N\}^T \{v_n\} \end{aligned} \tag{9}$$

For the 8-node quadrilateral, suitable polynomials that describe the appropriate variation of the sides can be written as:

$$\begin{aligned} x = \alpha_1 &+ \alpha_2 \xi + \alpha_3 \eta + \alpha_4 \xi^2 + \alpha_5 \eta\xi + \alpha_6 \eta^2 \\ &+ \alpha_7 \xi^2 \eta + \alpha_8 \eta^2 \xi \end{aligned} \tag{10}$$

or

$$x = [1, \xi, \eta, \xi^2, \xi\eta, \eta^2, \xi^2\eta, \eta^2\xi]\{\alpha_n\}$$

which ensures that on the sides where $\eta = \pm 1$ (see Figure 2.1), the variation may be up to quadratic in ξ, and likewise when $\xi = \pm 1$ the variation may be up to quadratic in η.

From (10) we can write:

$$\{x_n\} = [C]\{\alpha_n\} \tag{11}$$

or

$$\{\alpha_n\} = [C]^{-1}\{x_n\} \tag{12}$$

Or, in terms of the displacement functions we have:

$$[N_1, N_2, N_3 \ldots N_8] = [1, \xi, \eta, \xi^2, \eta\xi, \eta^2, \xi^2\eta, \eta^2\xi][C]^{-1} \tag{13}$$

Let ξ_i and η_i be the coordinate values of the i-th node in the normalized curvilinear system (ξ,η), then the displacement functions for the 8-node isoparametric quadrilateral are given by:

(a) For corner nodes: $i = 1, 3, 5, 7$

$$N_i = 1/4(1 + \xi\xi_i)(1 + \eta\eta_i)(\xi\xi_i + \eta\eta_i - 1) \tag{14}$$

(b) For midside nodes, $\xi_i = 0$: $i = 6$

$$N_i = 1/2(1 - \xi^2)(1 + \eta\eta_i) \tag{15}$$

(c) For midside nodes, $\eta_i = 0$: $i = 4,8$

$$N_i = 1/2(1 + \xi\xi_i)(1 - \eta^2) \tag{16}$$

2.2 Stiffness Matrix Formulation

To assemble the master stiffness matrix of a structural system, the element stiffness matrices are properly superimposed. Thus, we can write the master stiffness matrix as:

$$[K] = \sum_{i=1}^{m} [k_i] \tag{17}$$

where m = number of isoparametric elements and $[k_i]$ is the ith-element stiffness matrix defined by:

$$[k_i] = \int_A [B]^T[D][B]dA \tag{18}$$

with A here defined as the element area.

In the cartesian (x,y) system with corresponding displacement components (u,v), the components of strain in terms of displacements for linear elastic plane problems can be written as

$$\varepsilon_x = \frac{\partial u}{\partial x} \tag{19-a}$$

$$\varepsilon_y = \frac{\partial v}{\partial y} \tag{19-b}$$

and

$$\gamma_{xy} = \frac{\partial u}{\partial y} + \frac{\partial v}{\partial x} \tag{19-c}$$

In matrix form we may write:

$$\begin{Bmatrix} \varepsilon_x \\ \varepsilon_y \\ \gamma_{xy} \end{Bmatrix} = \begin{bmatrix} \frac{\partial}{\partial x} & 0 \\ 0 & \frac{\partial}{\partial y} \\ \frac{\partial}{\partial y} & \frac{\partial}{\partial x} \end{bmatrix} \begin{Bmatrix} u \\ v \end{Bmatrix} \tag{20}$$

Hence, for the element strain vector we write: for the isoparametric formulation

$$\{\varepsilon\} = [B]\{u\} \tag{21}$$

where:

$$[B] = [[B_1], [B_2], \ldots [B_m]] \tag{22}$$

being m the number of nodal points of the element

and,

$$\{u\} = \{u_1 \quad v_1 \quad u_2 \quad v_2 \ldots u_m \quad v_m\}^T$$

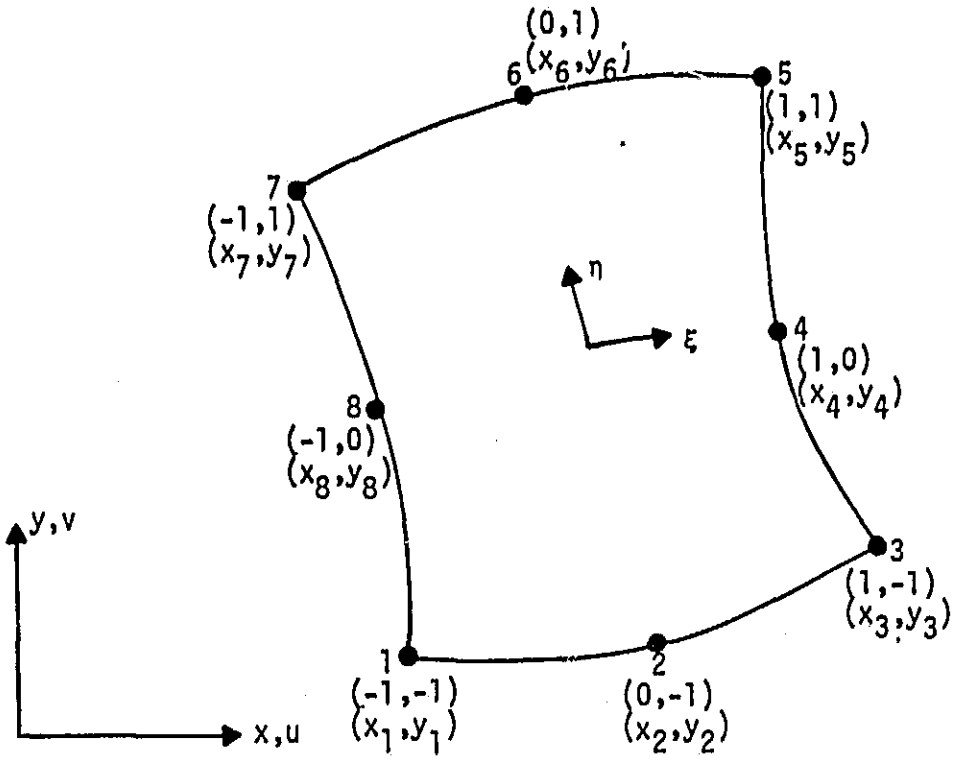

Figure 2.1

In terms of the displacement functions N_i, the matrices B_i can be written as:

$$[B_i] = \begin{bmatrix} \frac{\partial N_i}{\partial x} & 0 \\ 0 & \frac{\partial N_i}{\partial y} \\ \frac{\partial N_i}{\partial y} & \frac{\partial N_i}{\partial x} \end{bmatrix} \tag{23}$$

Since $N_i \equiv N_i(\xi,\eta)$, it is necessary to perform a coordinate transformation such that:

$$\frac{\partial N_i}{\partial x} = T_{x(\xi,\eta)} \cdot \frac{\partial N_i}{\partial \xi} \qquad \frac{\partial N_i}{\partial y} = T_{y(\xi,\eta)} \cdot \frac{\partial N_i}{\partial \eta} \tag{24}$$

where $T_{x(\xi,\eta)}$ and $T_{y(\xi,\eta)}$ are vector transformation functions relating x and ξ, and y and η, respectively.

In terms of the local coordinates we may write then,

$$\begin{Bmatrix} \frac{\partial N_i}{\partial \xi} \\ \frac{\partial N_i}{\partial \eta} \end{Bmatrix} = \begin{bmatrix} \frac{\partial x}{\partial \xi} & \frac{\partial y}{\partial \xi} \\ \frac{\partial x}{\partial \eta} & \frac{\partial y}{\partial \eta} \end{bmatrix} \begin{Bmatrix} \frac{\partial N_i}{\partial x} \\ \frac{\partial N_i}{\partial y} \end{Bmatrix} = [J] \begin{Bmatrix} \frac{\partial N_i}{\partial x} \\ \frac{\partial N_i}{\partial y} \end{Bmatrix} \tag{25}$$

where [J] is the Jacobian matrix*, which can also be written in terms of the global cartesian coordinates as:

$$[J] = \begin{bmatrix} \frac{\partial N_1}{\partial \xi}, & \frac{\partial N_2}{\partial \xi}, \ldots, & \frac{\partial N_m}{\partial \xi} \\ \frac{\partial N_1}{\partial \eta}, & \frac{\partial N_1}{\partial \eta}, \ldots, & \frac{\partial N_m}{\partial \eta} \end{bmatrix} \begin{Bmatrix} x_1 & y_1 \\ x_2 & y_2 \\ x_i & y_i \\ \cdot & \cdot \\ \cdot & \cdot \\ x_m & y_m \end{Bmatrix} \tag{26}$$

where $\{x_i\}$, $\{y_i\}$ are the global coordinates of the element nodes.

Now we may write:

$$\begin{Bmatrix} \frac{\partial N_i}{\partial x} \\ \frac{\partial N_i}{\partial y} \end{Bmatrix} = [I][J]^{-1} \begin{Bmatrix} \frac{\partial N_i}{\partial \xi} \\ \frac{\partial N_i}{\partial \eta} \end{Bmatrix} \tag{27}$$

where I is the identity matrix,

$$[I] = \begin{bmatrix} 1 & 0 \\ 0 & 1 \end{bmatrix}$$

In equation (20) all the derivatives,

$$\frac{\partial N_i}{\partial \xi} \quad \text{and} \quad \frac{\partial N_i}{\partial \xi}$$

can be obtained by hand from the original displacement functions N_i for the particular type of element being used (see Appendix A).

*Note that independently of the number of element nodes [J] is always a 2×2 matrix, for two-dimensional problems.

Once (26) and (27) are calculated we may substitute after some manipulation into (25) and obtain the B_i's. Thereafter, the matrix [B] can be assembled.

Having [B] in terms of the normalized local curvilinear coordinates (ξ,η), we must express the element of area in (18) in terms of the local coordinates ξ and η.

Consequently, we write

$$dA = dxdy = |J|\, d\eta d\xi \tag{28}$$

and because we have used normalized local coordinates, the limits of integration are now -1 and 1 for both integrals. Thus, we obtain the element stiffness matrix in the form:

$$[k_i] = \int_{-1}^{1}\int_{-1}^{1} [B(\xi,\eta)]^T[D][B(\xi,\eta)]\ |J|\ d\xi d\eta \tag{29}$$

2.3 Numerical Integration Procedure

The difficulties of performing a closed form area integration for the element stiffness matrix (29) are avoided by use of numerical integration techniques. For elastic problems the closed form integration is tedious; for elasto-plastic problems, impossible, as in this case the constitutive matrix is not available in closed form. Before attempting any numerical integration, it is a requirement to know the degree of accuracy needed to ensure stability and convergence to the correct result.

If the internal element forces due to internal element stresses can be determined exactly by numerical integration for a constant state of stresses within each element, we can guarantee convergence to the correct solution. This argument has been discussed in detail by Irons [6], Zienkiewicz [1], and others.

The interelement forces can be expressed as:

$$\{f\} = \left(\int_A [B]^T[D][B]dA\right)\{u\} \tag{30}$$

Or in terms of the stresses:

$$\{f\} = \int_A [B]^T\{\sigma\}dA \tag{31}$$

Thus, by numerical integration, we must be able to determine exactly such intergrals as

$$\int_{-1}^{1}\int_{-1}^{1} \frac{\partial N}{\partial x}\,|J|\,d\xi d\eta$$

obtained by combining equations (27) and (28).

The integration using Gauss-Legendre quadrature is highly simplified because of the constant boundary values (-1, +1) that the local normalized curvilinear coordinates take in each element.

According to Gauss-Legendre quadrature [5] we may write the element stiffness matrix given by (29) in the form:

$$[k] = \sum_{k=1}^{m}\sum_{\ell=1}^{m} C_k C_\ell [B(\xi_k,\eta_\ell)]^T[D][B(\xi_k,\eta_\ell)]\,|J| \tag{32}$$

where C_k, C_ℓ are the coefficients of the integration points k and ℓ.

$[B(\xi_k,\eta_\ell)]^T$ and $[B(\xi_k,\eta_\ell)]$ are the matrices evaluated at the Gauss point (ξ_k,η_ℓ), and m is the number of integration points used.

In [1] it is argued that 2×2 Gauss quadrature provides an exact numerical evaluation of the element stiffness of the 8-node quadrilateral, independent of the activated terms in the displacement functions. This is true in tension and shear problems where only terms as high as ξ^3 are present in (32) once the internal product is performed. It has been documented [7] that 2×2 Gauss quadrature is exact only when terms

as high as cubic are present in the product form of (32). Several exercises performed during the development of ISOFINEL and its subsequent testing, showed that in problems such as pure shear, pure bending, three point bending, etc., with elements having a large slenderness ratio, much more accurate answers are obtained when using 3×3 Gauss quadrature.

The program in its actual version contains both features, at the user's option, both to facilitate the work discussed in this report and for possible subsequent usage.

3. SOLUTION PROCEDURE

The master stiffness matrix [K] in (18) is a square, symmetric and positive-definite matrix. The solution of the linear equations related to the finite element analysis takes a large fraction of the total CPU time. Furthermore, the storage space occupied by the complete matrix is sometimes so large that medium size problems are insoluble if access to tapes or peripherial storage is not provided. However, at this point, we are interested in saving storage at the expense of time.

The master stiffness in structural problems is banded when precautions have been taken in the nodal numbering scheme. Therefore, the storage of the complete matrix is unnecessary and is avoided by assembling K in a rectangular form at the same time it is constructed. The number of rows may correspond to the number of equations to be solved, and the number of columns equal to the maximum semi-bandwidth.

Before proceding to solve the system of equations, the boundary conditions are applied. In the actual version, admissible boundary conditions are the following:

- prescribed non-zero nodal displacements in the x-direction
- prescribed non-zero nodal displacements in the y-direction
- prescribed nodal forces in the x-direction
- prescribed nodal forces in the y-direction
- zero nodal displacements in the x or y direction.

The program makes use of the Gauss elimination procedure [6] to solve for the nodal displacements of the expression

$$\{F\} = [K]\{\delta\}$$

4. PROGRAM STRUCTURE

The ISOFINEL computer code has been developed having in mind two major premises. First, the main body of the program should remain intact once plasticity is implemented. For this reason, some parts have been partitioned into different subroutines that at first glance would look superfluous. Second, eventually the same program will host special crack-tip elements for the elasto-plastic analysis of stress fields at the vicinity of cracks. Thus, many parameters, such as number of element nodes, number of Gaussian integration points, etc., have been left in terms of variables subject to be changed via input.

In the following pages a flow diagram of the main program and its subroutines is presented. It is not the purpose here to expand into the particular aspects of the coding; some diagrams of subroutines whose contents are self-explanatory are omitted.

4.1 ISOFINEL: Main Program

4.1.1 Description of Terms:

NEL = number of elements

NPROB = number of problems

ICONT = actual problem number (from 1 to NPROB).

NRD = total number of degrees of freedom.

4.1.2 Description of Subroutines Not Accompanied by Flow Diagrams:

START: Reads material properties- geometry, dimensions, boundary conditions, etc., and print them.

ZEROS: Initialize arrays for

(a) Stiffness Matrix, [K]

(b) Derivatives Matrix, [B]

(c) Displacement Vector, {δ}

(d) Force Vector, {F}

DISFUN: Contains in explicit form the shape functions and their derivatives. Calculates them at Gaussian integration points for either the 2x2 G.I. option or the 3×3 G.I.

STRSTR: Calculates the elements of the elasticity matrix, D, for either the case of plane stress or plane strain.

BOUCO: Applies boundary conditions and modifies master stiffness matrix such that is in the correct form for the solution procedure. Possible boundary conditions are:

- prescribed x or y nodal displacements
- prescribed x or y nodal forces
- zero nodal displacements.

GAUSEL: Solves for the nodal displacements by using the Gauss Elimination Procedure.

NODFOR: Performs the matrix multiplication

$$[K]\ \{\delta\}$$

to return the generalized nodal forces.

OUTPUT: Prints out all information:

(a) Nodal Displacements, {δ}

(b) Nodal Forces, {F}

(c) Strains at Gauss Points, {ε}

(d) Stresses at Gauss Points, {σ}

(e) Stresses and Strains at the Elements Centroid

(f) Principal Stresses

(g) Coordinates (x,y) of Gauss Points

(h) Execution time of Each Subroutine.

4.2 Flow Diagram

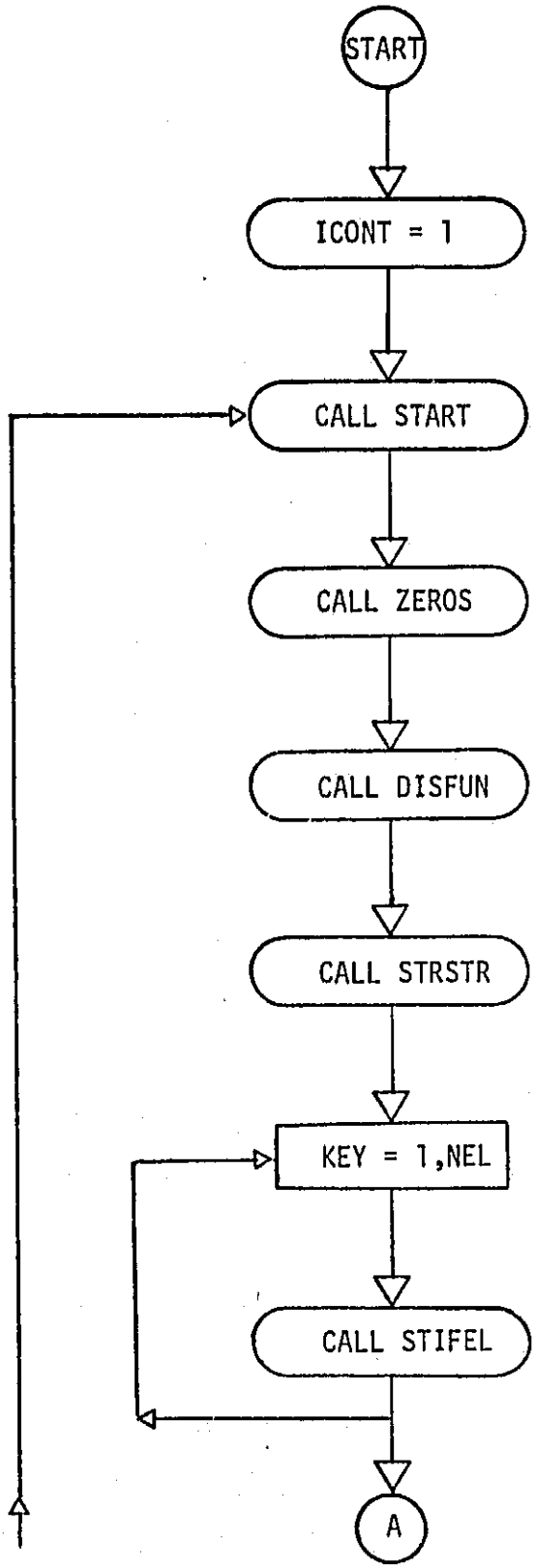

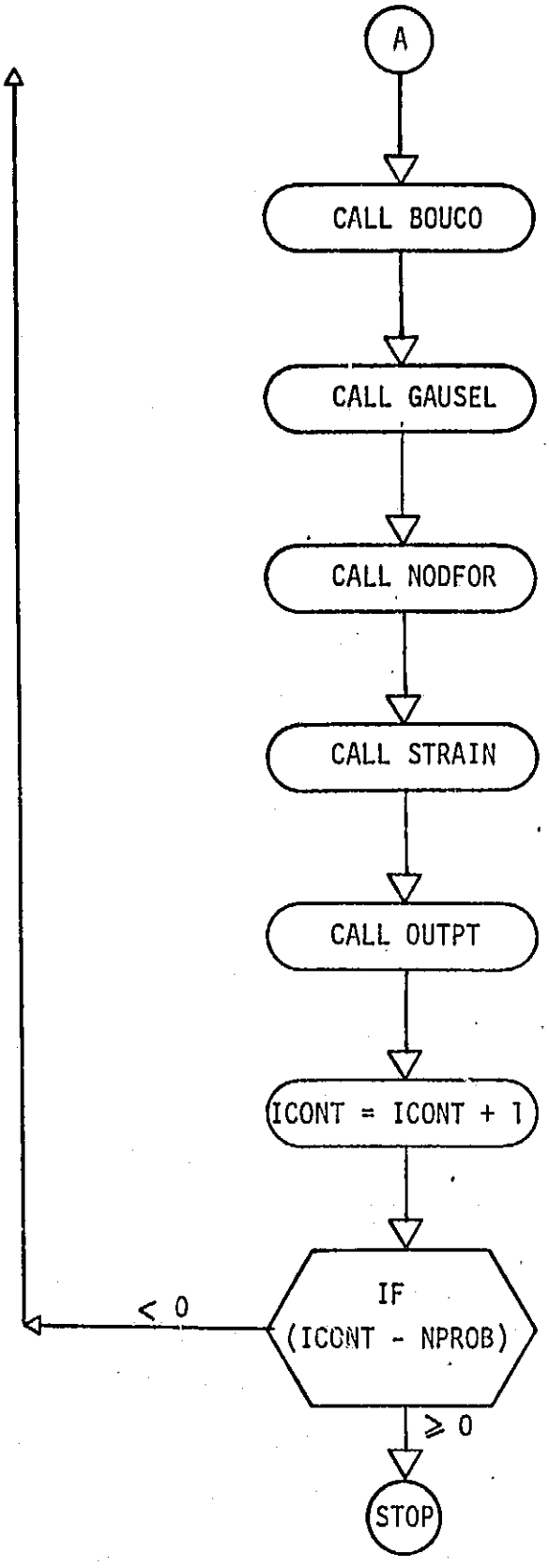
A
CALL BOUCO
CALL GAUSEL
CALL NODFOR
CALL STRAIN
CALL OUTPT
ICONT = ICONT + 1
IF
(ICONT - NPROB)
< 0
≥ 0
STOP

4.3 STIFEL: Stiffness Matrix Subroutine

4.3.1 Description of Terms:

NGA2 = 9 for 3x3 Gauss integration; 4 for 2x2 Gauss integration

NEL8 = NEL*8

NOEL = number of nodes for element (8, for present case)

NDF = number of degrees of freedom per node (2, for present case)

NBW = Bandwidth of master stiffness matrix

INOEL = NRD*NOEL

NM(I) = array of nodal configuration, (I = 1, NEL8)

XYM(J) = array of nodal coordinates, (J = 1, NRD)

XJAC(I,J) = Jacobian matrix, (I = 1,2; J = 1,2)

DDF(L,K) = array of derivatives of displacement functions, (L = 1, NGA2; K = 1, INOEL)

BM(I,J,K,L) = array for B-matrix, (I = 1, NEL; J = 1,2: K = 1, NOEL; L = 1, NGA2)

TEMPK(I,J) = array for element stiffness matrix, (I = 1, INOEL; J = 1, INOEL)

STIF(K,L) = array for master stiffness matrix, (K = 1, NRD; L = 1, NBW)

4.3.2 Description of Subroutine Not Accompanied by a Flow Diagram

MATMUL: Performs the matrix multiplication $[B]^T[D][B]$ and returns the upper symmetric part of the element stiffness matrix.

4.4 Flow Diagram

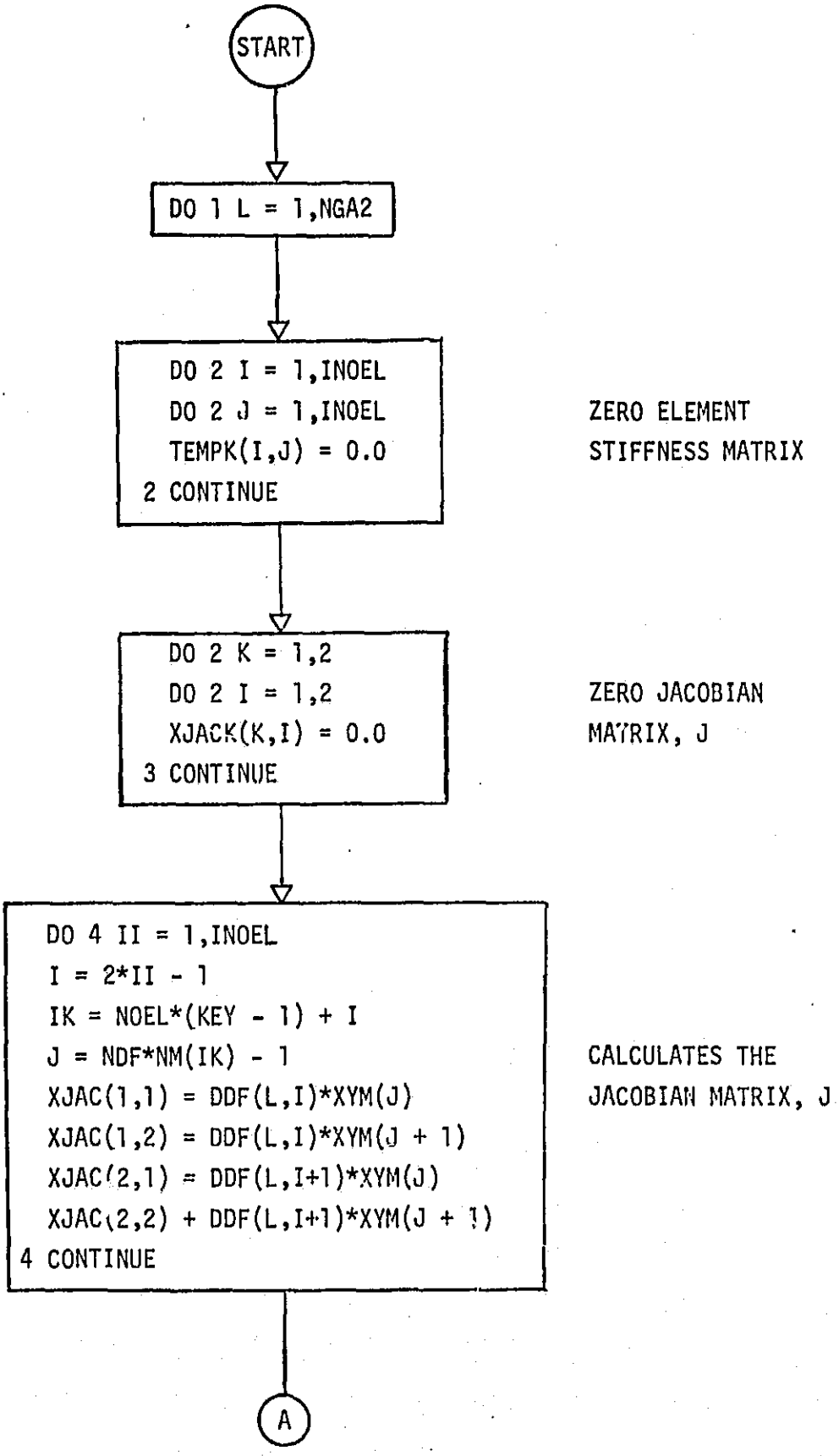

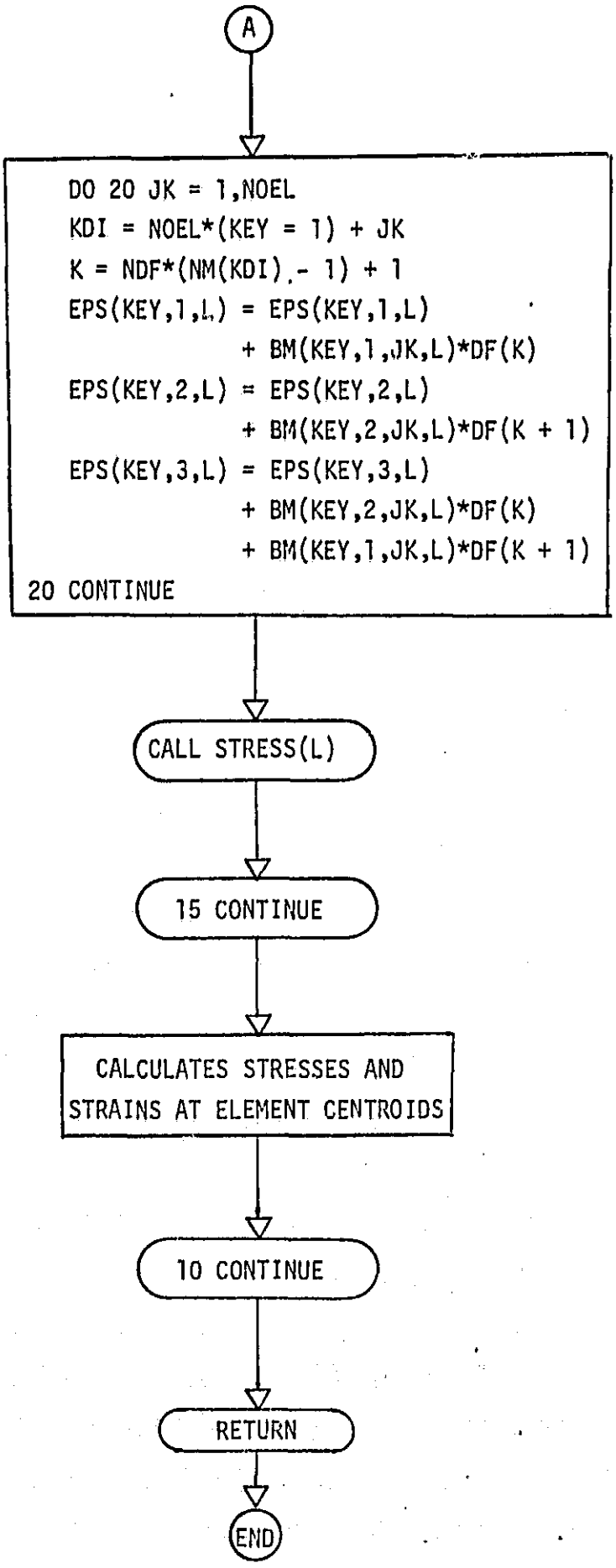
A
DO 20 JK = 1,NOEL
KDI = NOEL*(KEY = 1) + JK
K = NDF*(NM(KDI) - 1) + 1
EPS(KEY,1,L) = EPS(KEY,1,L)
+ BM(KEY,1,JK,L)*DF(K)
EPS(KEY,2,L) = EPS(KEY,2,L)
+ BM(KEY,2,JK,L)*DF(K + 1)
EPS(KEY,3,L) = EPS(KEY,3,L)
+ BM(KEY,2,JK,L)*DF(K)
+ BM(KEY,1,JK,L)*DF(K + 1)
20 CONTINUE
CALL STRESS(L)
15 CONTINUE
CALCULATES STRESSES AND
STRAINS AT ELEMENT CENTROIDS
10 CONTINUE
RETURN
END

4.5 STRAIN: Strains and Stresses Subroutine

4.5.1 Description of Terms:

EPS(I,J,K) = Array of strains, $\varepsilon_x, \varepsilon_y, \gamma_{xy}$, (I = 1,NEL; J = 1.3; K = 1,NGA2)

SIG(I,J,K) = Array of stresses, $\sigma_x, \sigma_y, \tau_{xy}$, (I = 1,NEL; J = 1,3; K = 1,NGA2)

DF(L) = Array of nodal displacements, (L = 1,NRD)

4.6 Flow Diagram

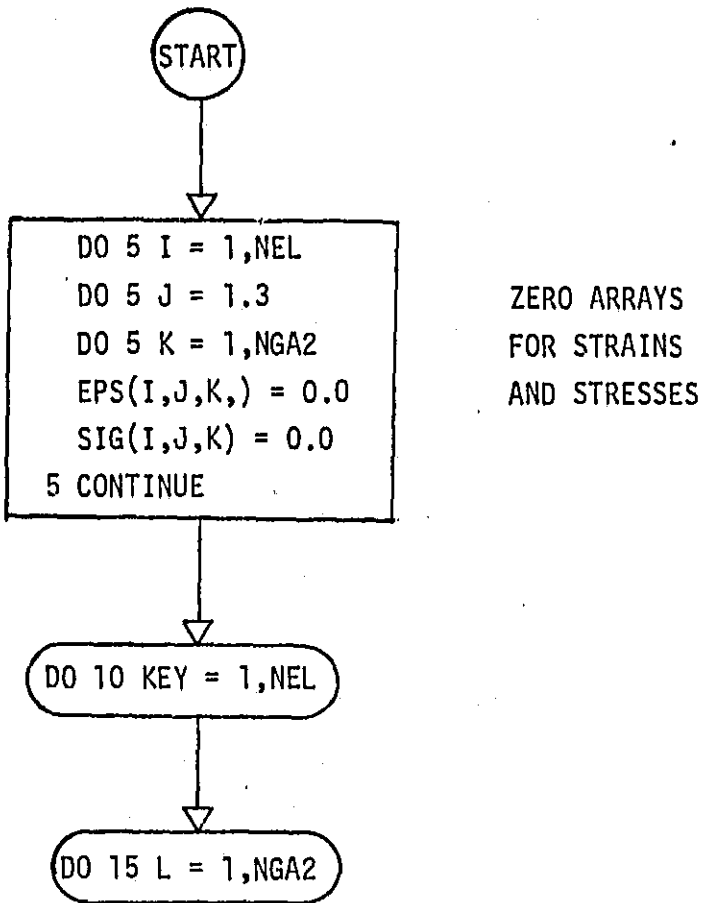

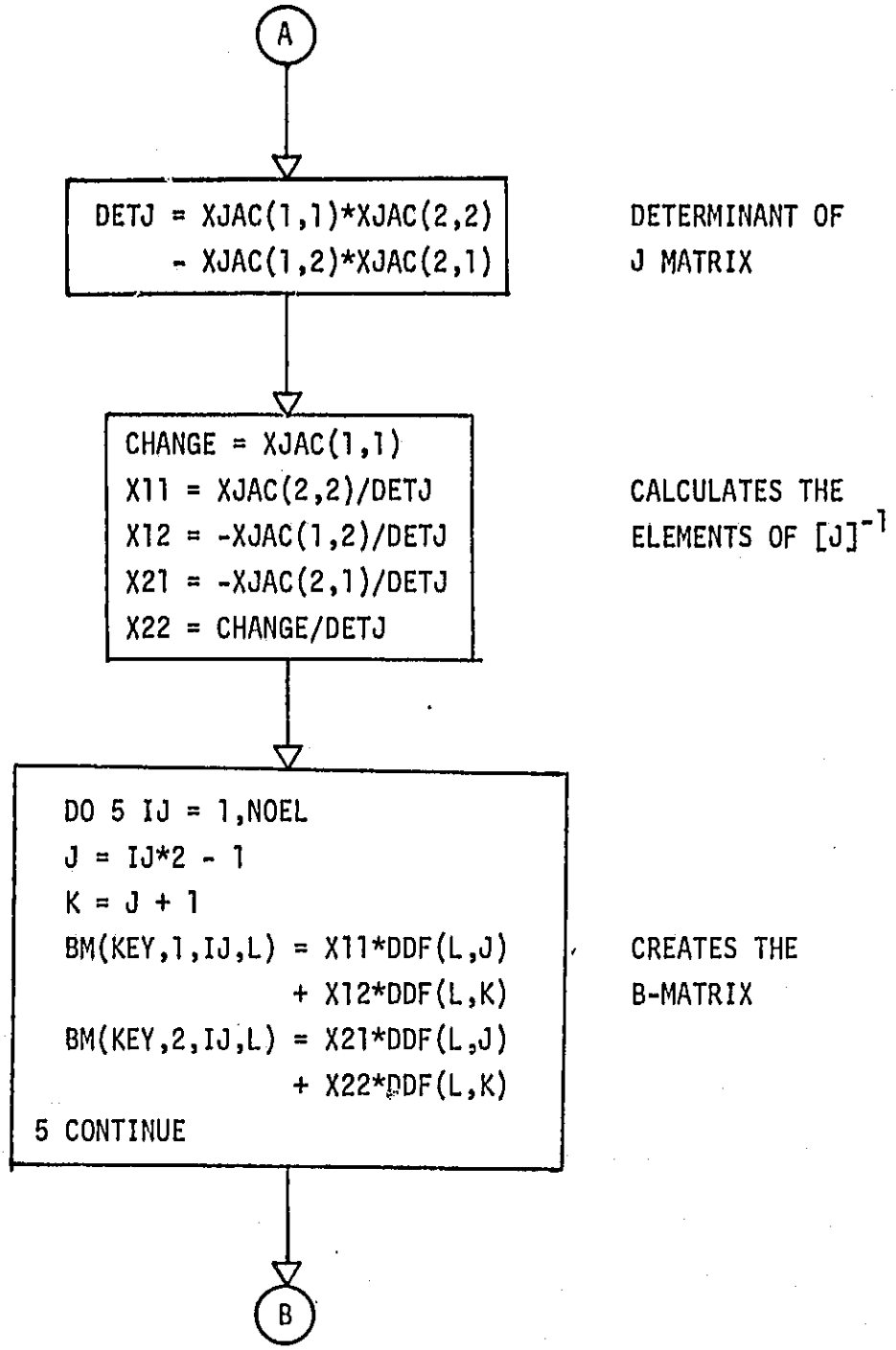
A
DETJ = XJAC(1,1)*XJAC(2,2)
- XJAC(1,2)*XJAC(2,1)
DETERMINANT OF
J MATRIX
CHANGE = XJAC(1,1)
X11 = XJAC(2,2)/DETJ
X12 = -XJAC(1,2)/DETJ
X21 = -XJAC(2,1)/DETJ
X22 = CHANGE/DETJ
CALCULATES THE
ELEMENTS OF [J]-1
DO 5 IJ = 1,NOEL
J = IJ*2 - 1
K = J + 1
BM(KEY,1,IJ,L) = X11*DDF(L,J)
+ X12*DDF(L,K)
BM(KEY,2,IJ,L) = X21*DDF(L,J)
+ X22*DDF(L,K)
5 CONTINUE
CREATES THE
B-MATRIX
B

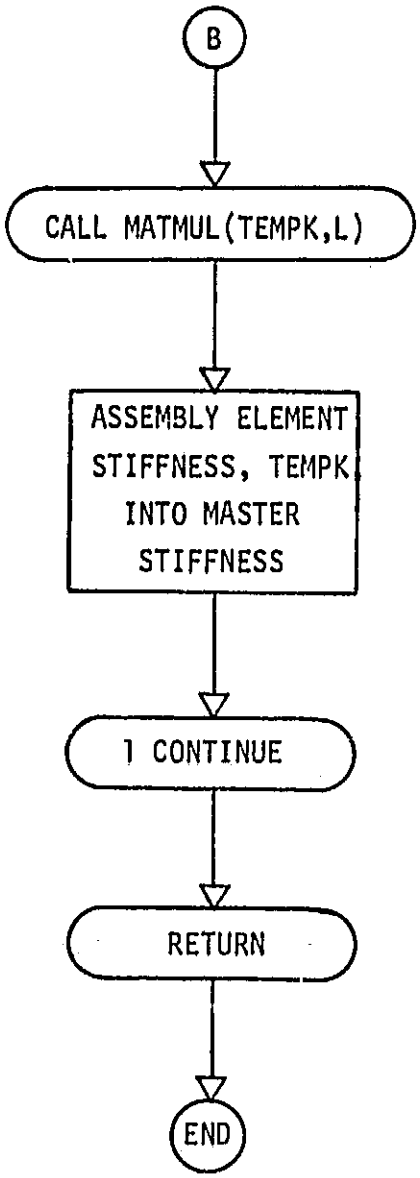
B
CALL MATMUL(TEMPK,L)
ASSEMBLY ELEMENT STIFFNESS, TEMPK INTO MASTER STIFFNESS
1 CONTINUE
RETURN
END

5. NUMERICAL RESULTS

To test the capability and limitations of the program, two problems are solved:

- Uniaxial Tension
- Pure Shear
- Pure Bending

They are solved using both 2×2 and 3×3 Gauss integration. As it was described earlier, the displacement and strain solutions of these problems are contained in the shape functions of the eight-node isoparametric quadrilateral. Hence, it is expected that they may be solved exactly by a single element.

Three different maps containing 1,4 and 10 elements are tested. Each map is tested for three different element sizes. Figure 5.1 shows the configuration of each map.

5.1 Uniaxial Tension

The uniaxial tension problem is solved by prescribing uniform y-displacements at the nodes on the surface $y = L$, and by preventing vertical motion of the nodes on the surface $y = 0$. Being the solution of this problem contained in the displacement functions of the element, it is not strictly necessary to prevent rigid body motion. However, it is done by restraining the middle node at the origin to move. For all maps, the prescribed displacements correspond to 1% of the original length of the plate. The solutions obtained for both displacements and stresses are in excellent agreement (less than 0.001% error) with the expected theoretical values. No differences are observed between the two integration procedures studied.

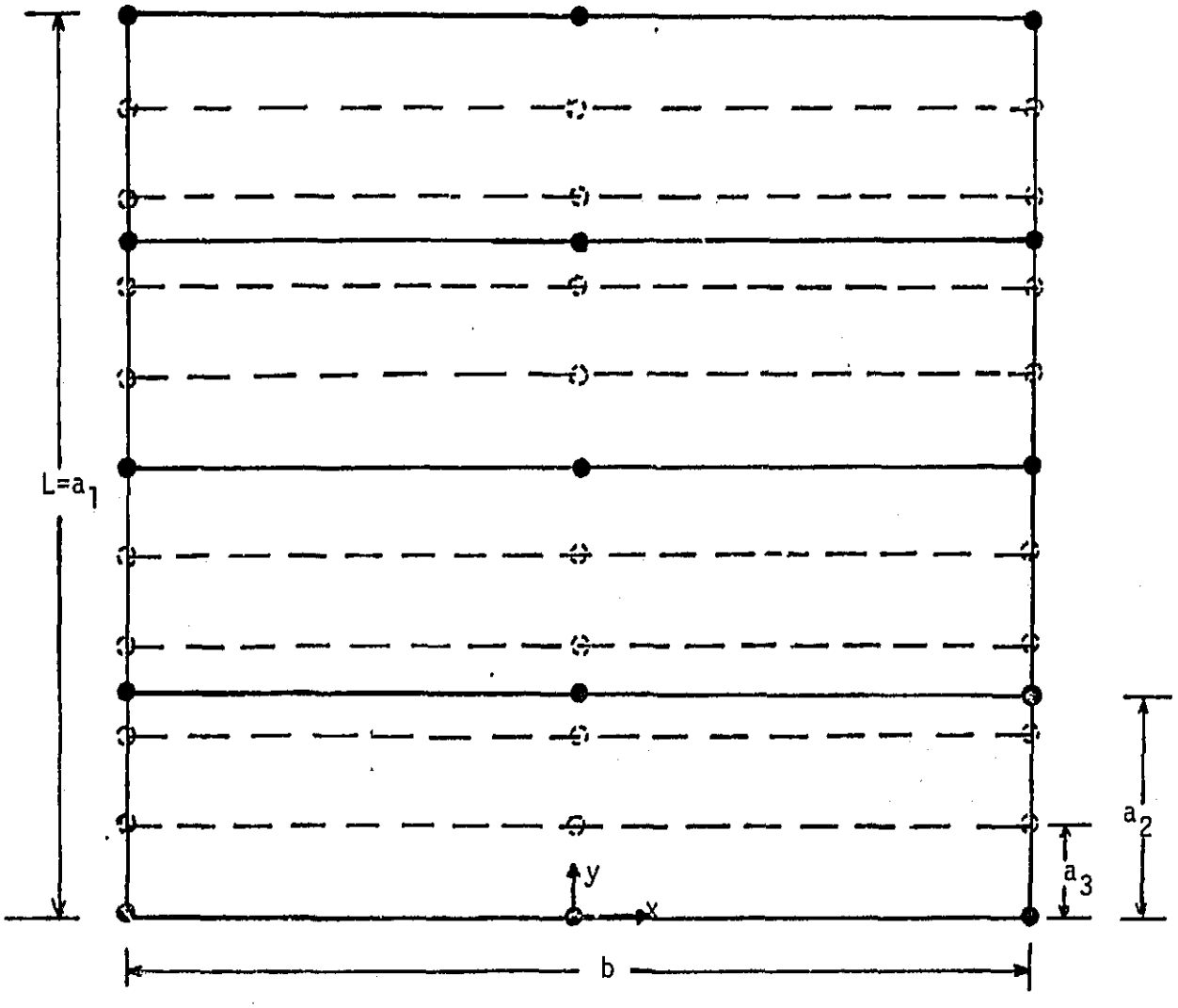

MAP 1 (Outer Quadrangle)		MAP 2 (———)			MAP 3 (- - - - - -)		
Case	a_1/b	Case	a_2/b	L/b	Case	a_3/b	L/b
1A	1.0	2A	0.25	1.0	3A	0.1	1.0
1B	10.0	2B	2.50	10.0	3B	1.0	10.0
1C	20.0	2C	5.00	20.0	3C	2.0	20.0

Figure 5.1

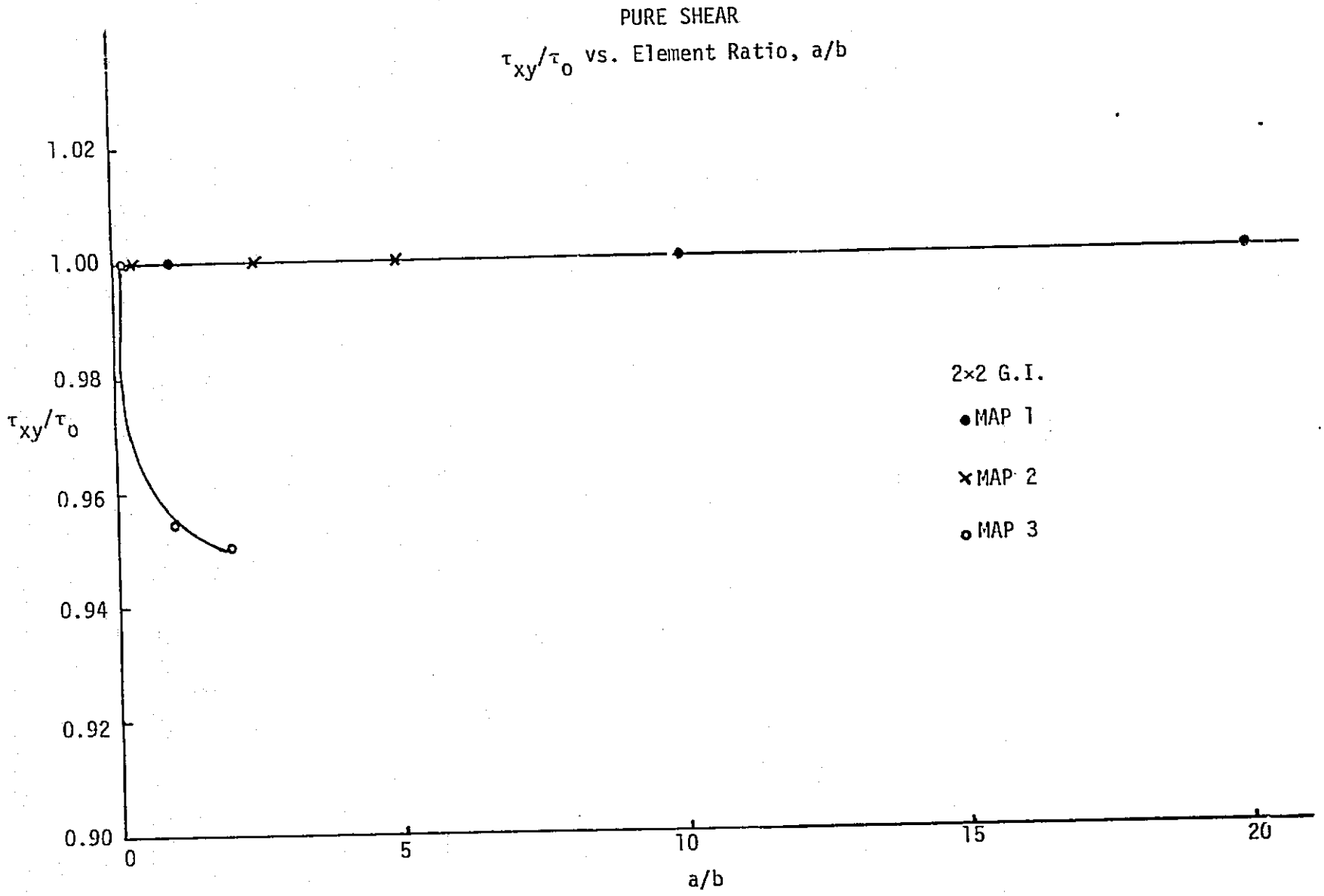
PURE SHEAR
τ_{xy}/τ_o vs. Element Ratio, a/b
1.02
1.00
0.98
0.96
0.94
0.92
0.90
τ_{xy}/τ_o
0
5
10
15
20
a/b
2×2 G.I.
MAP 1
MAP 2
MAP 3

Figure 5.2

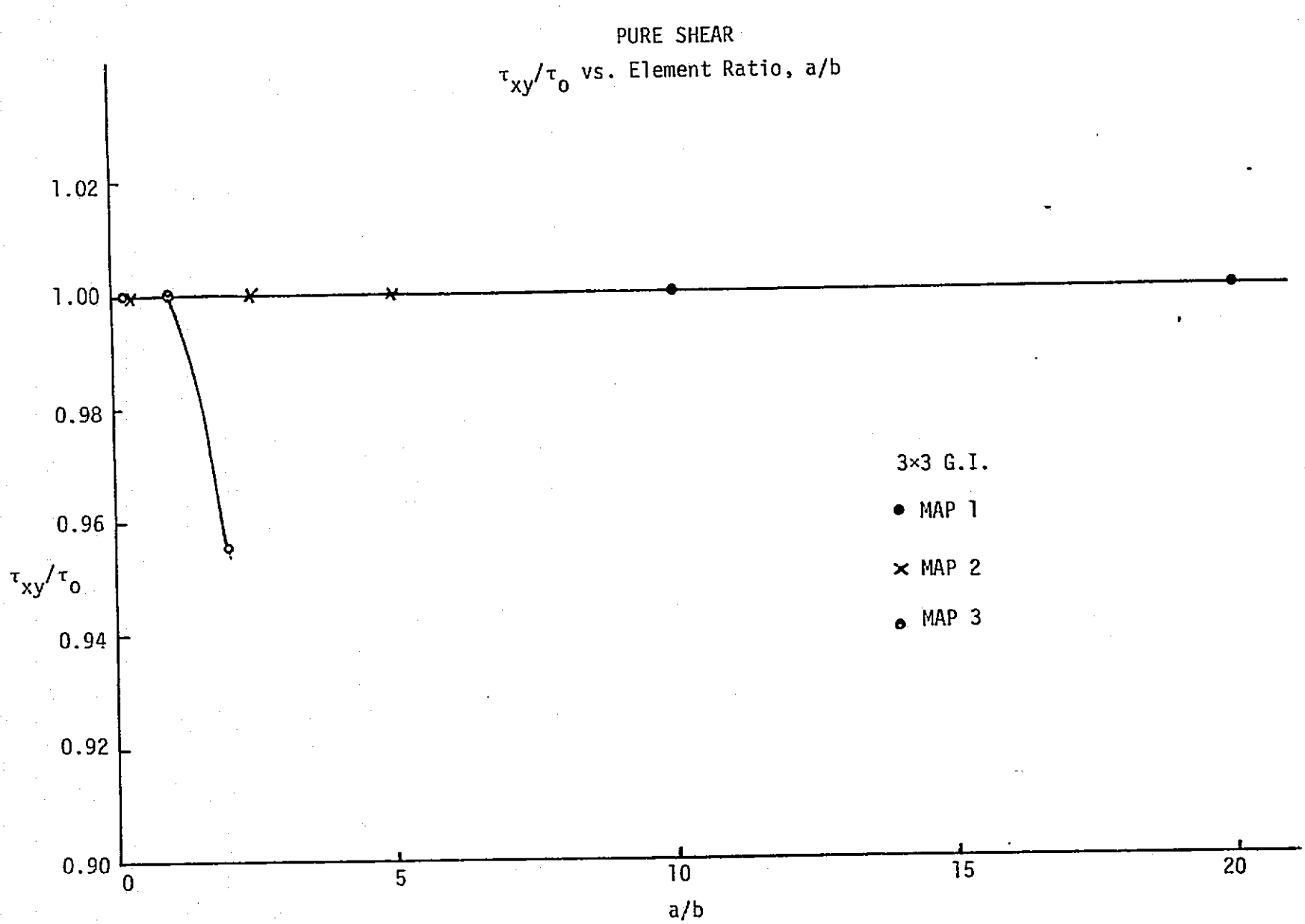
PURE SHEAR
τ_{xy}/τ_o vs. Element Ratio, a/b
1.02
1.00
0.98
0.96
0.94
0.92
0.90
τ_{xy}/τ_o
0
5
10
15
20
a/b
3×3 G.I.
MAP 1
MAP 2
MAP 3

Figure 5.3

5.2 Pure Shear

The pure shear problem is solved by prescribing linear varying x-displacements at the boundary nodes. The x-displacements are given by the relation,

$$\delta_x = (y/L)\delta_0$$

where δ_0 is the displacement prescribed on the surface $y = L$. For each map, δ_0 is 1% of the plate length, L.

Several results are studied, Figures 5.2 and 5.3 show the variation of the normalized shear stress, (τ_{xy}/τ_0), with τ_0 being the theoretical stress, versus the element ratio (a/b), for the 2×2 and 3×3 Gauss integration procedures, respectively. The value of τ_{xy} chosen for each case is that at the Gauss point that differs more from the theoretical value. Values at Gauss points very close to the surface, where horizontal displacements are prescribed, are not taken in consideration because of local effects. These effects are only detected in Map 3, where Gauss points are closer to the boundaries, but they die out rapidly. Maps 2 and 3 present excellent agreement in both cases, being negligible the difference between the two integration procedures. However, for Map 3, Case C, there is a large improvement when 3×3 G.I. is used, since for an element ratio of a/b = 1.0 there is a 4.25% error in stresses in the 2×2 G.I. compared with a 0.001% error in the 3×3 G.I. When a/b = 2.0, the errors are 5 and 4.25%, respectively. Figures 5.4 to 5.7 present the variation of the normalized shear stress along the direction perpendicular to the plane of shear for a constant x/b. The value of x/b is determined by the position of the integration points within each element. In this case, x/b attains the values of 0.2887 and 0.3873 for the 2×2 and 3×3 G.I. procedures, respectively.

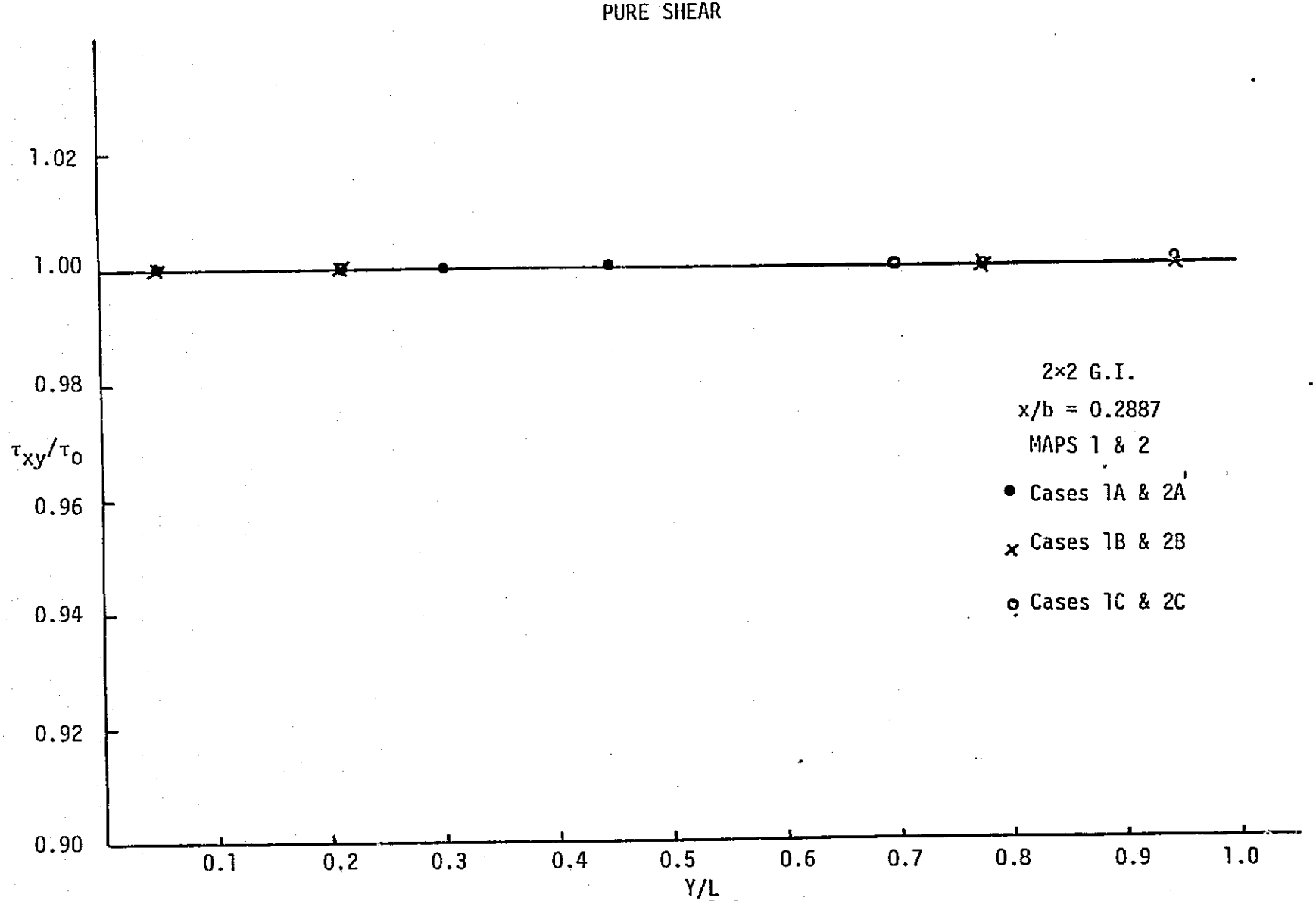
PURE SHEAR
1.02
1.00
0.98
0.96
0.94
0.92
0.90
τ_{xy}/τ_o
0.1
0.2
0.3
0.4
0.5
0.6
0.7
0.8
0.9
1.0
Y/L
2×2 G.I.
x/b = 0.2887
MAPS 1 & 2
Cases 1A & 2A
Cases 1B & 2B
Cases 1C & 2C

Figure 5.4

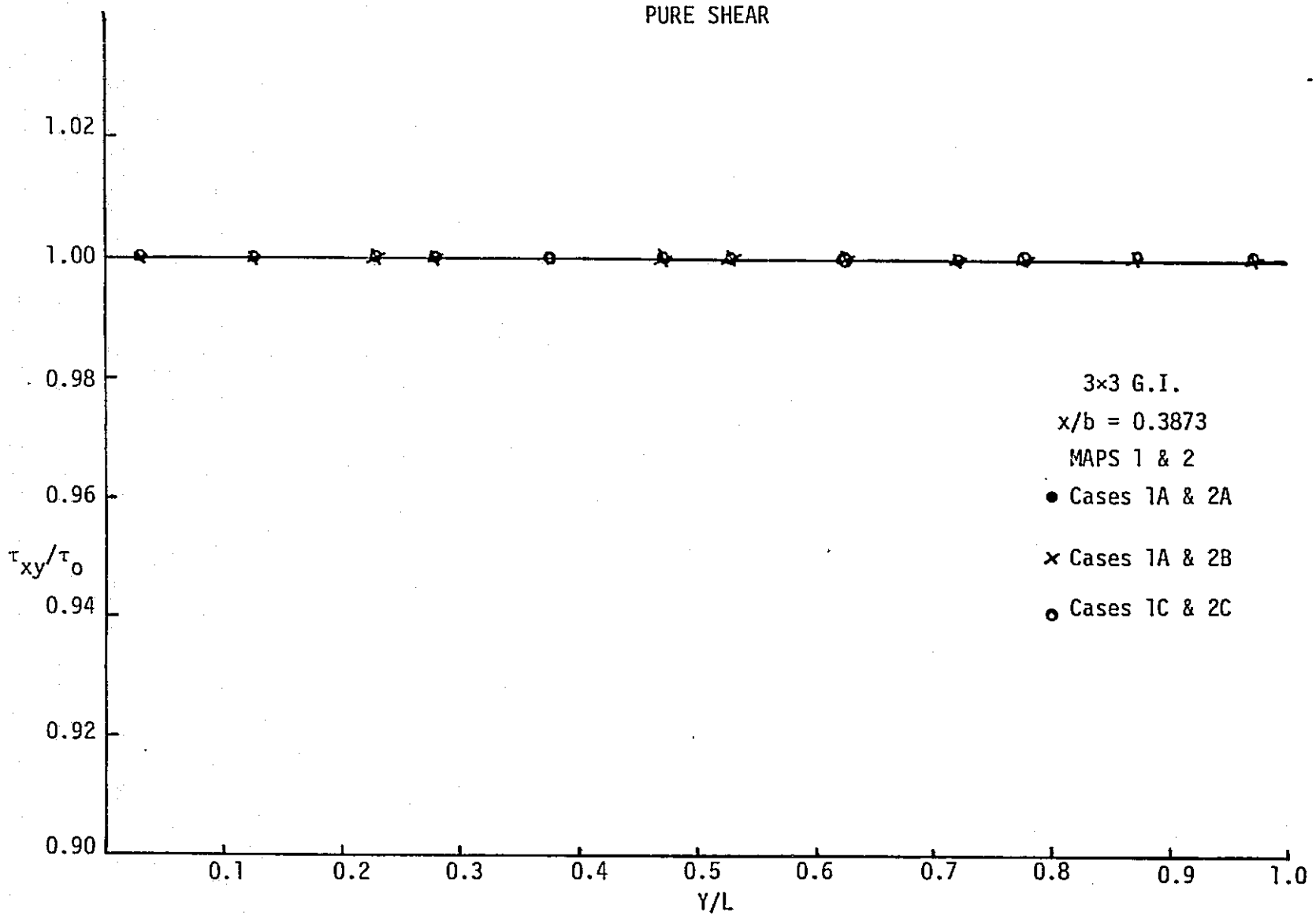
PURE SHEAR
1.02
1.00
0.98
0.96
0.94
0.92
0.90
τ_{xy}/τ_o
0.1
0.2
0.3
0.4
0.5
0.6
0.7
0.8
0.9
1.0
Y/L
3×3 G.I.
x/b = 0.3873
MAPS 1 & 2
● Cases 1A & 2A
× Cases 1A & 2B
o Cases 1C & 2C

Figure 5.5

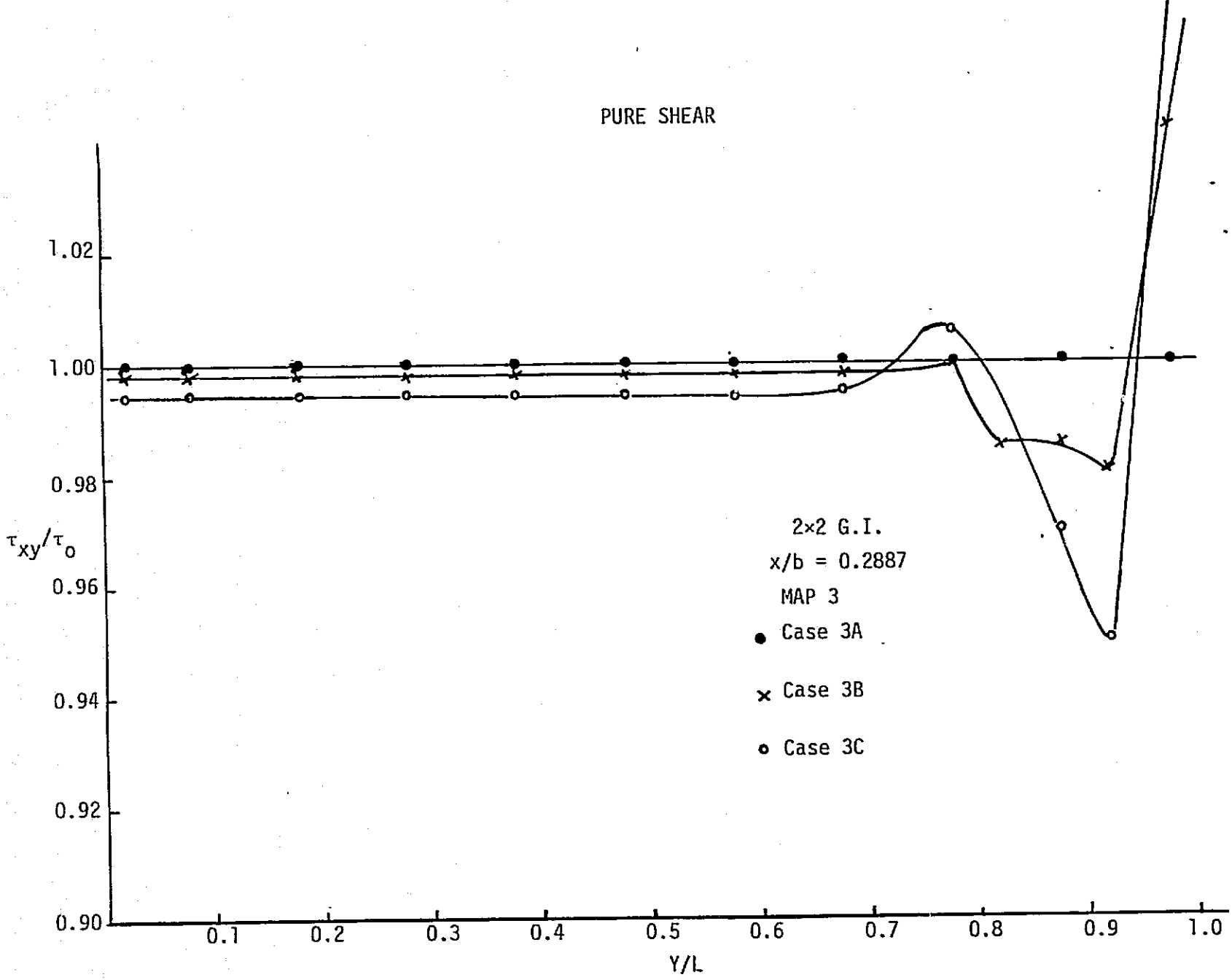
PURE SHEAR
1.02
1.00
0.98
0.96
0.94
0.92
0.90
τ_{xy}/τ_o
2×2 G.I.
x/b = 0.2887
MAP 3
Case 3A
Case 3B
Case 3C
0.1
0.2
0.3
0.4
0.5
0.6
0.7
0.8
0.9
1.0
Y/L

Figure 5.6

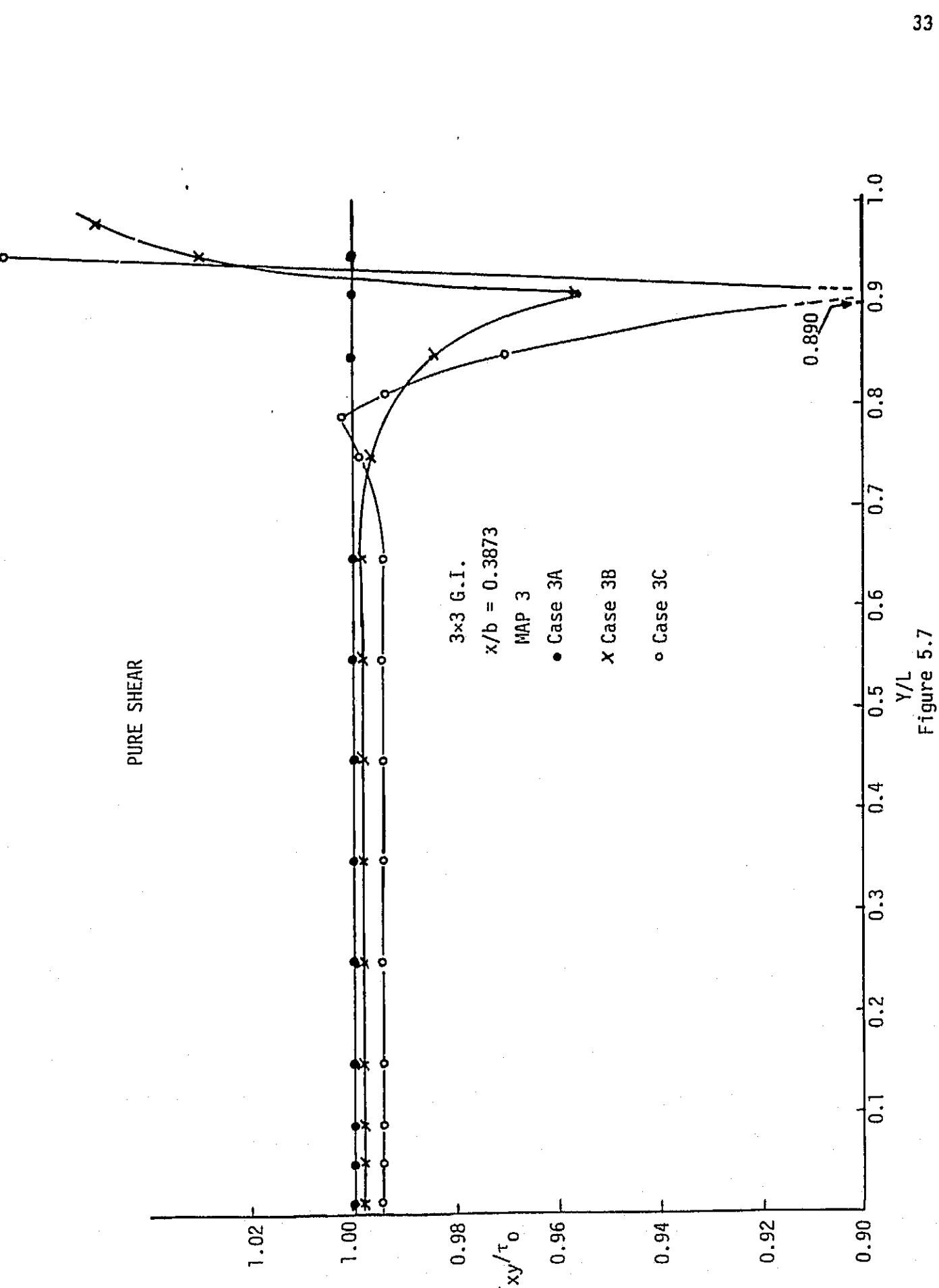
PURE SHEAR
3×3 G.I.
x/b = 0.3873
MAP 3
• Case 3A
X Case 3B
∘ Case 3C
0.890
τ_{xy}/τ_o
1.02
1.00
0.98
0.96
0.94
0.92
0.90
0.1
0.2
0.3
0.4
0.5
0.6
0.7
0.8
0.9
1.0
Y/L

Figure 5.7

Maps 1, 2 and Case 3A of Map 3 provide solutions that are in excellent agreement with the existing solution. Neglecting the error introduced by the local effects at the plane of shear, the error in the shear stress for cases 3B and 3C is summarized in Table 5.1 below.

Case	2×2 G.I.		3×3 G.I.	
	Max. Error	Mean Error	Man. Error	Mean Error
3B	1.4%	0.2%	1.5%	0.2%
3C	2.0%	0.6%	3.0%	0.6%

Table 5.1

It is observed that both procedures produce highly comparable results with a slight advantage of the 2×2 G.I. In this particular problem, the difference is due more to the numerical error introduced by the larger number of operations that take place in the assembling of the stiffness matrix in the 3×3 G.I. case.

As it is known from the theoretical solution, the stresses σ_x and σ_y are both zero for the case of pure shear. However in the numerical computation, the true value of these stresses is related among others to the element ratio, numerical integration scheme, and of course type of displacement functions used. In the present case we are interested only in the former two. Figures 5.8 and 5.9 are plots of the variation of the "amplified zero-stress" along the axis perpendicular to the plane of shear. The numerical values of σ_x are chosen arbitrarily since the values obtained for σ_y are comparable. An amplification of 10^3 is chosen, since from the engineering viewpoint any pair of stresses with a difference in order of magnitude below this quantity is usually considered. From these two graphs

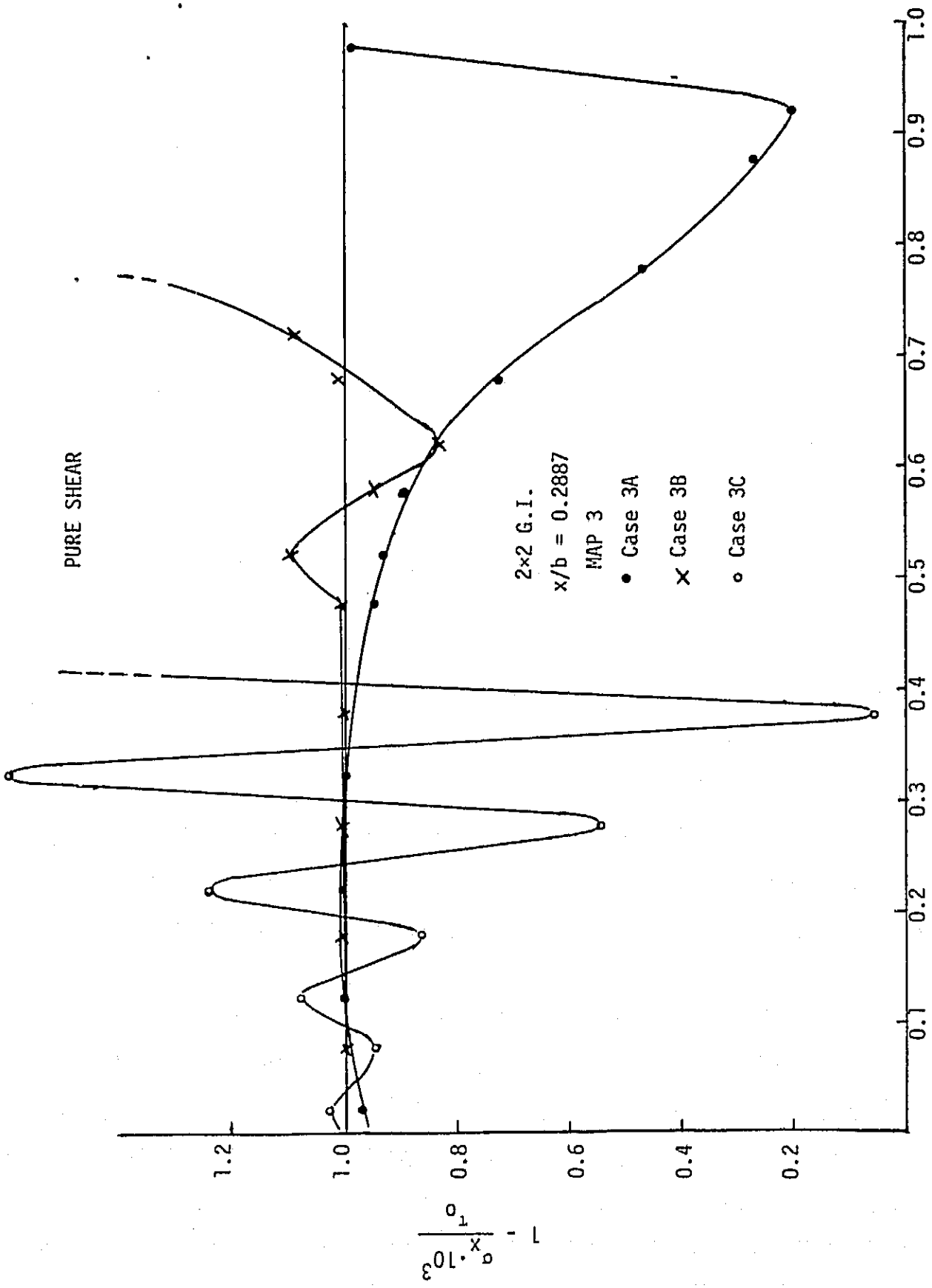
PURE SHEAR
2×2 G.I.
x/b = 0.2887
MAP 3
• Case 3A
× Case 3B
∘ Case 3C
1 - σx·10³ / τo
Y/L
1.2
1.0
0.8
0.6
0.4
0.2
0.1
0.2
0.3
0.4
0.5
0.6
0.7
0.8
0.9
1.0

Figure 5.8

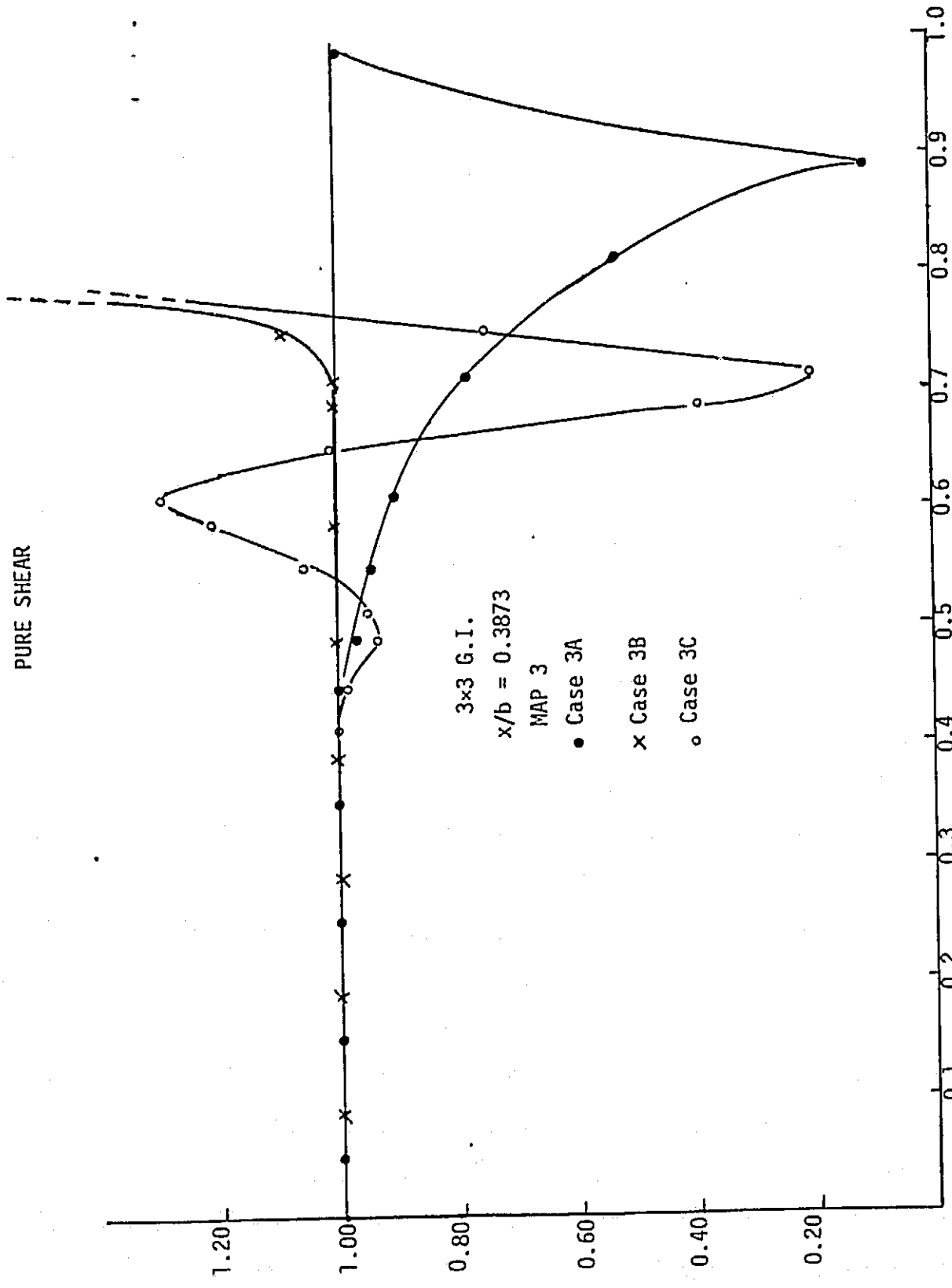
PURE SHEAR
3×3 G.I.
x/b = 0.3873
MAP 3
• Case 3A
× Case 3B
∘ Case 3C
1 - σx·10³/τo
Y/L
1.20
1.00
0.80
0.60
0.40
0.20
0.1
0.2
0.3
0.4
0.5
0.6
0.7
0.8
0.9
1.0

Figure 5.9

it is appreciated the advantage of using 3×3 G.I. in more complex problems. Figure 5.8 shows for the 2×2 G.I. scheme, Cases 3A and 3B, that half distance away from the plane of shear the "assumed-zero stresses" start increasing in magnitude even that before being one-fourth of plate length close to the plane of shear have already attained values comparable to the shear stress. For Case 3C the same phenomena is observed well before a section half plate length away from the plane of shear. When the 3×3 G.I. scheme is used, this effect disappears in the first half section of the plate and is highly reduced in the rest.

5.3 Pure Bending

The pure bending problem is solved by applying linear varying y-displacements on the surface $y = L$ with a line of symmetry at $x = 0$. The prescribed displacements are given by

$$\delta_y = (x/b)\delta_o$$

where δ_o is the displacement prescribed at the corner nodes and corresponds to 1% of the plate length. Figures 5.10 and 5.11 show a variation of the normalized bending stress (σ_y/σ_o) with the element ratio for the 2×2 and 3×3 G.I. schemes respectively. It is observed that by performing a 3×3 G.I., the stress results improve enormously for Maps 1 and 2, but little is gained on Map 3. Figures 5.12 and 5.13 present the variation of the bending stress along the axial direction of the plate for Map 1. Although the maximum error in stress is only about 1.3% for the Case 1C of 2×2 G.I., the error is reduced to 0.001% when 3×3 G.I. is used (Figure 5.13). Similar results are observed in Figures 5.14 to 5.17 for Maps 2 and 3. It is observed, however, that by moving to a 3×3 G.I., the improvement in the stresses is only of the order of 40%. These results are summarized in Table 5.2.

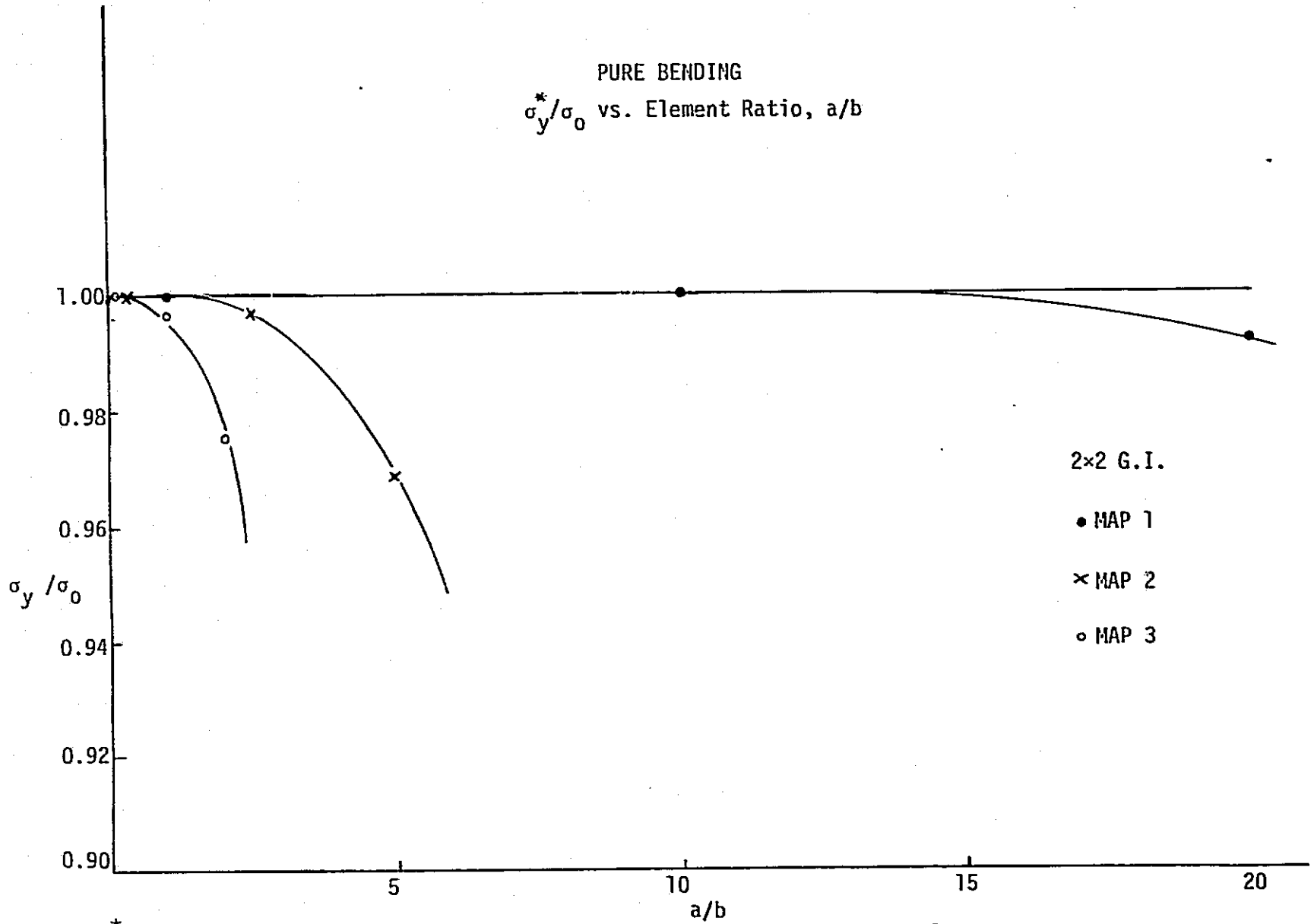

$^*\sigma_y$ chosen is that at Gauss Point differing more from theoretical value.

Figure 5.10

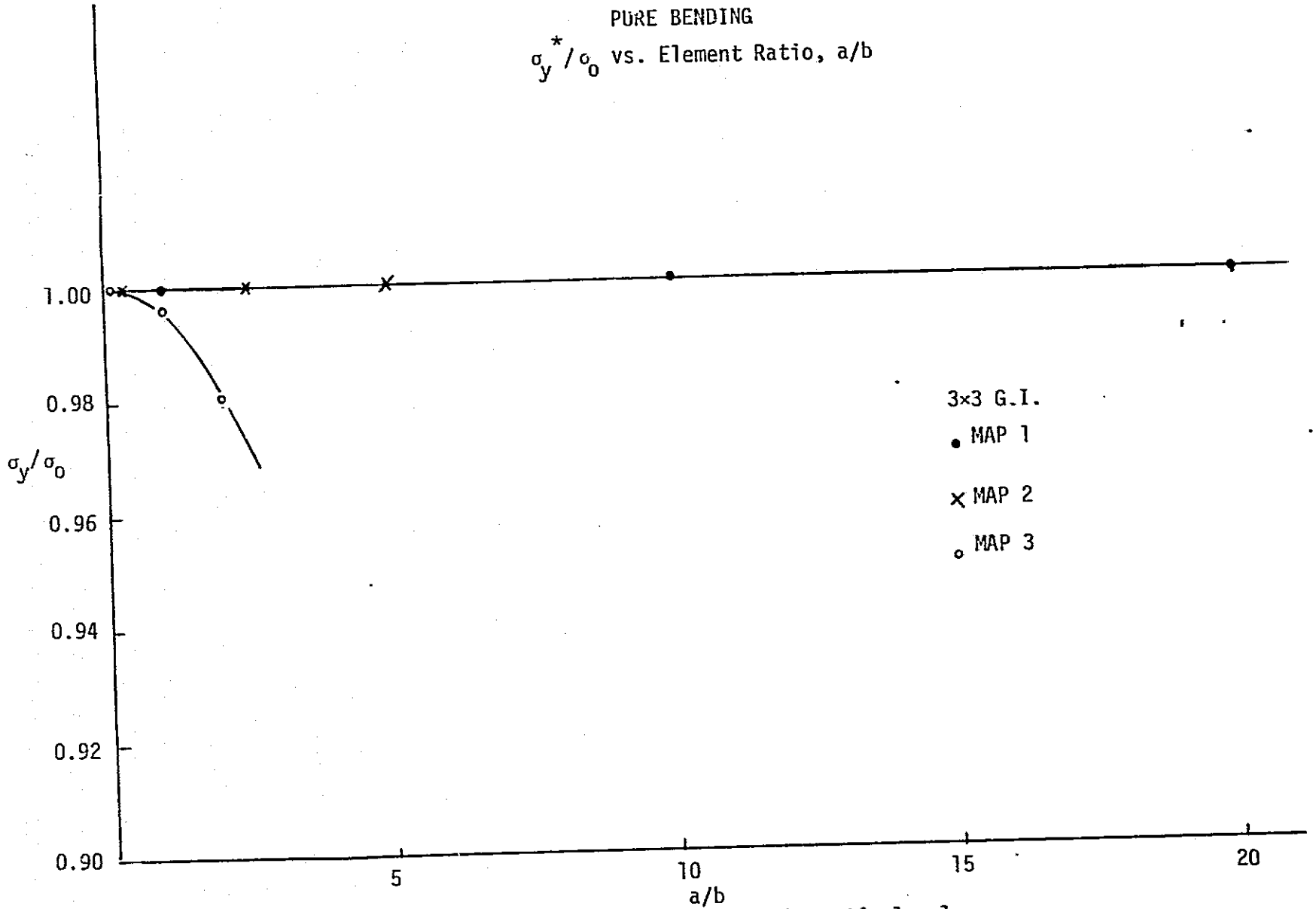

$^*\sigma_y$ chosen is that at Gauss Point differing more from theoretical value.

Figure 5.11

PURE BENDING

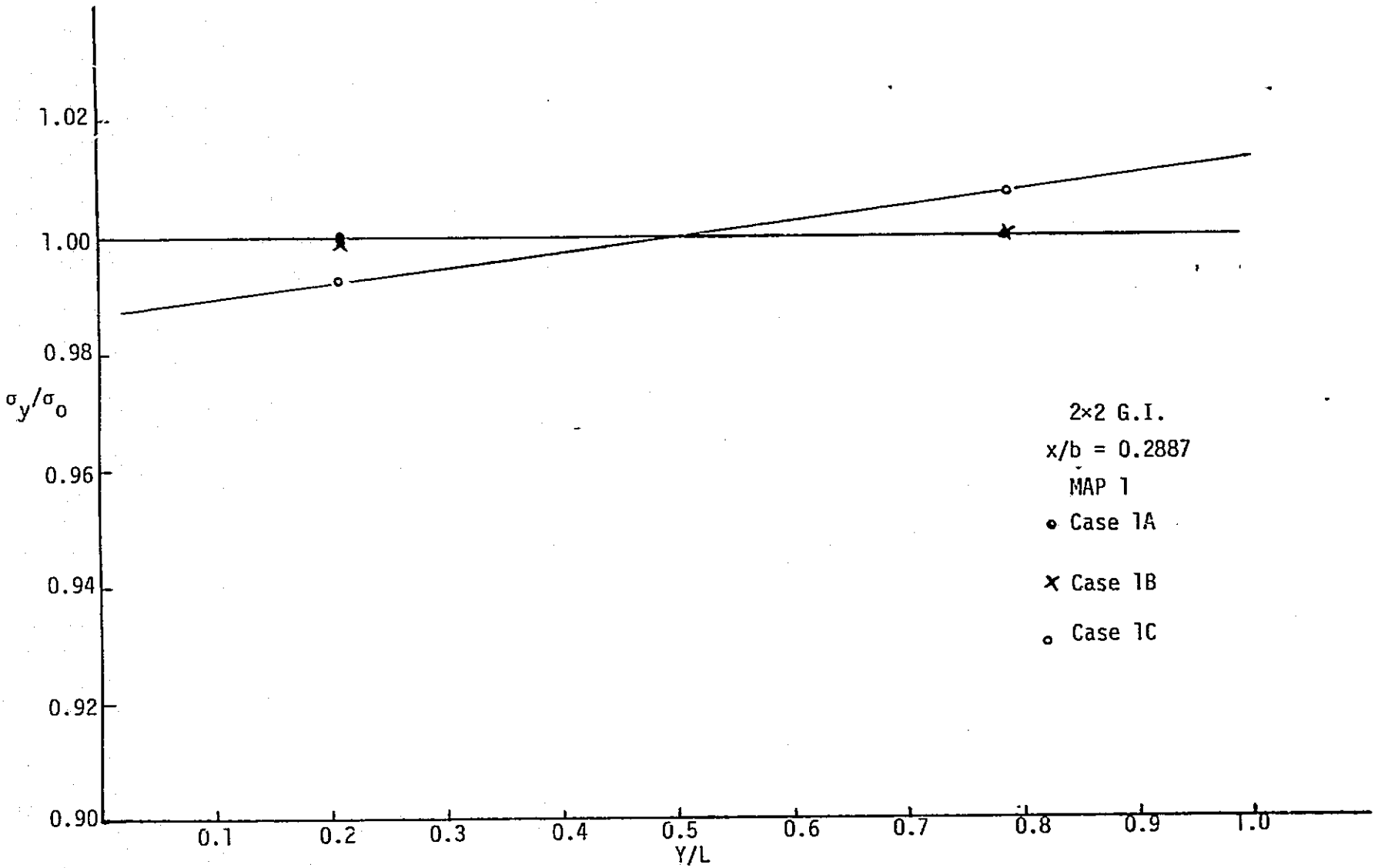

Figure 5.12

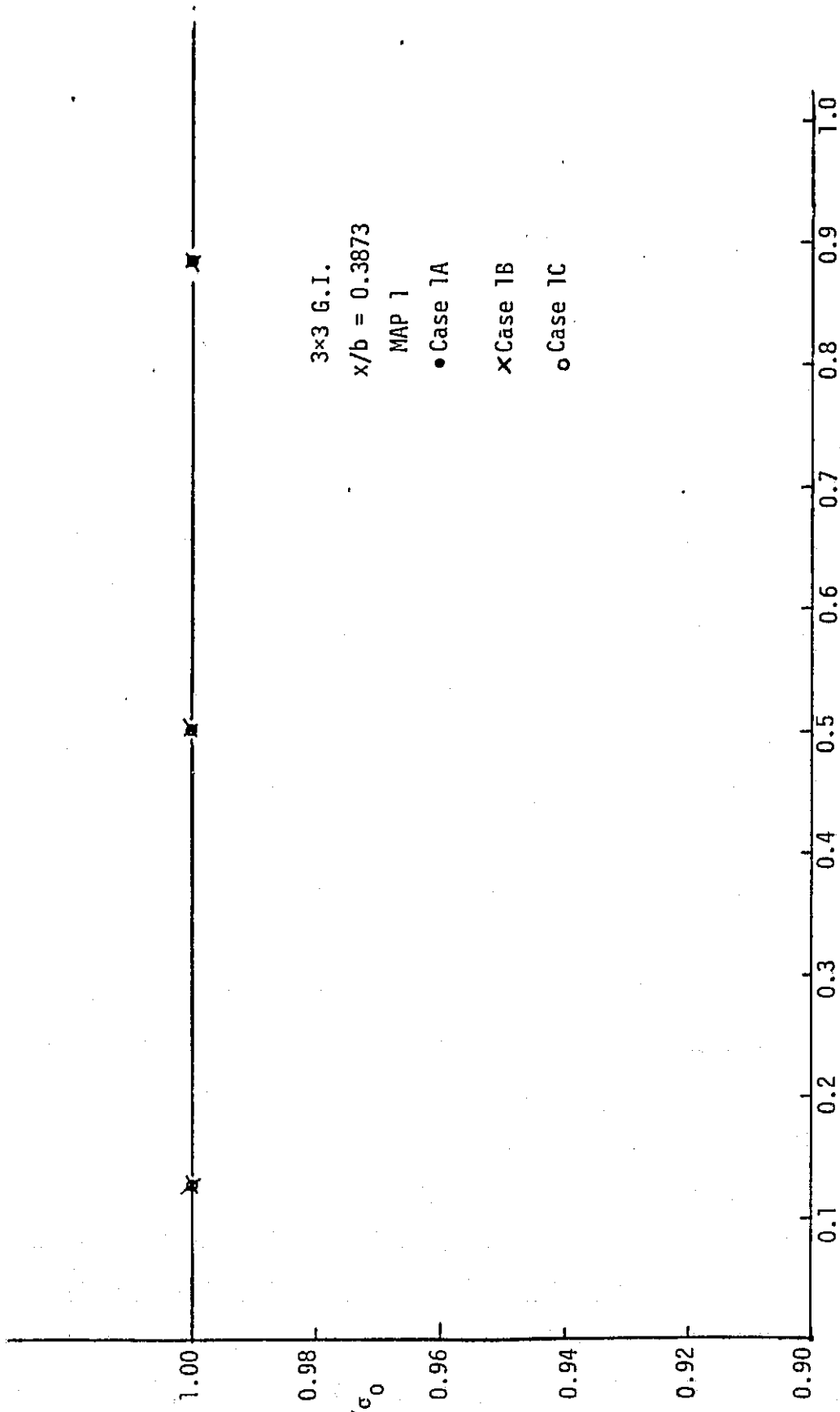
PURE BENDING
3×3 G.I.
x/b = 0.3873
MAP 1
• Case 1A
× Case 1B
o Case 1C
σ_y/σ_o
1.00
0.98
0.96
0.94
0.92
0.90
0.1
0.2
0.3
0.4
0.5
0.6
0.7
0.8
0.9
1.0
Y/L

Figure 5.13

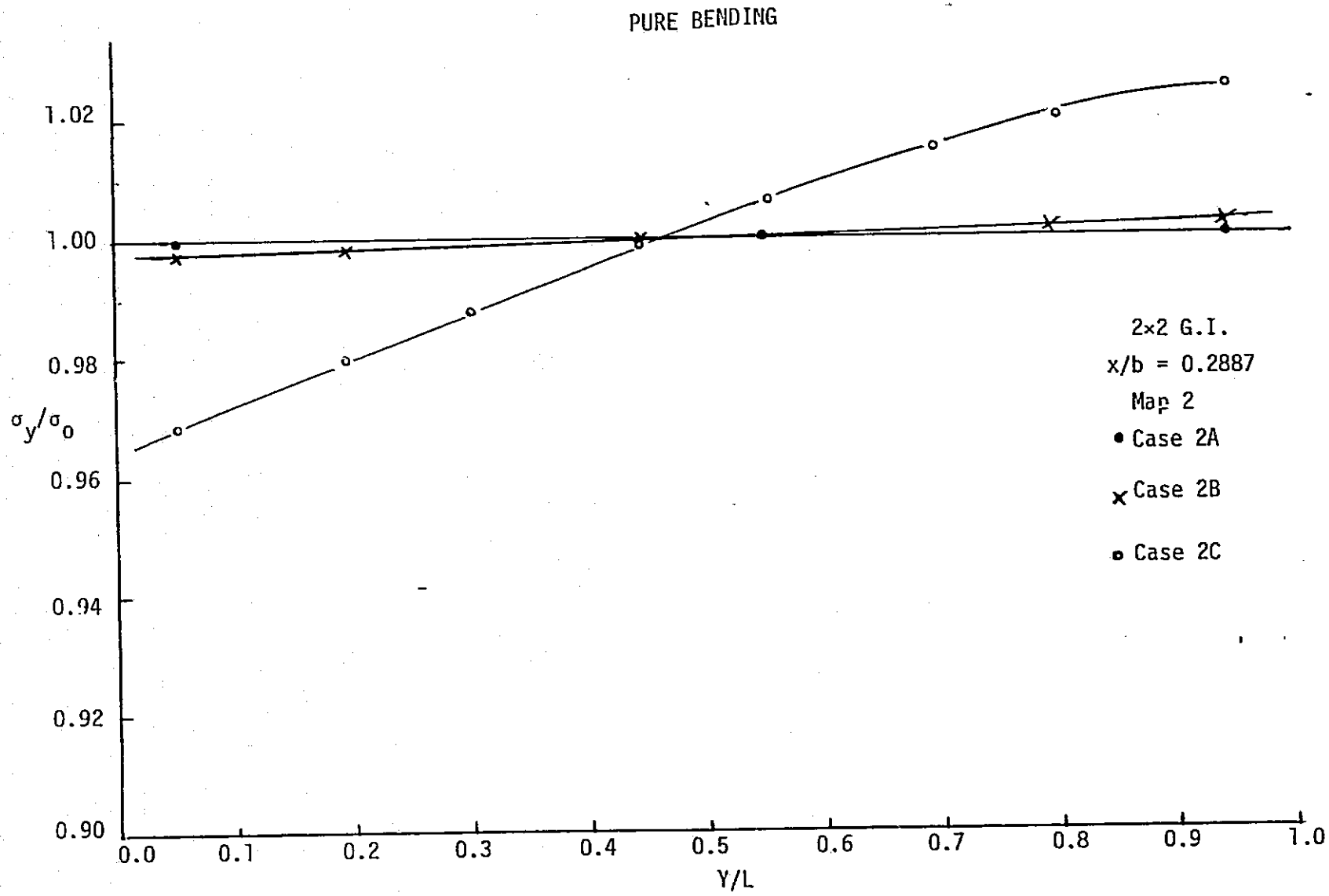
PURE BENDING
1.02
1.00
0.98
0.96
0.94
0.92
0.90
σ_y/σ_o
0.0
0.1
0.2
0.3
0.4
0.5
0.6
0.7
0.8
0.9
1.0
Y/L
2×2 G.I.
x/b = 0.2887
Map 2
Case 2A
Case 2B
Case 2C

Figure 5.14

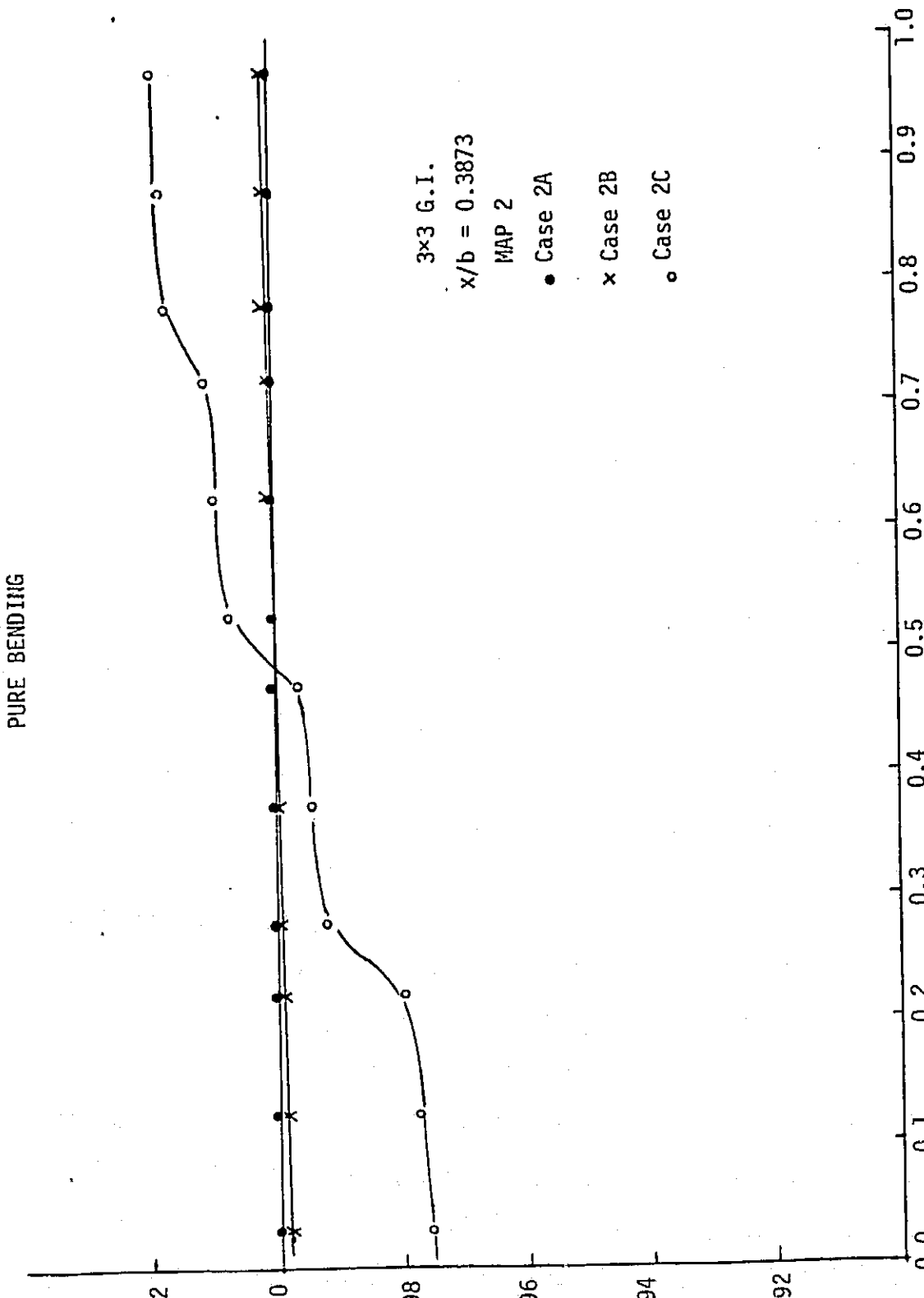
PURE BENDING
3×3 G.I.
x/b = 0.3873
MAP 2
• Case 2A
× Case 2B
o Case 2C
σ_y/σ_o
1.02
1.00
0.98
0.96
0.94
0.92
0.0
0.1
0.2
0.3
0.4
0.5
0.6
0.7
0.8
0.9
1.0
Y/L

Figure 5.15

PURE BENDING

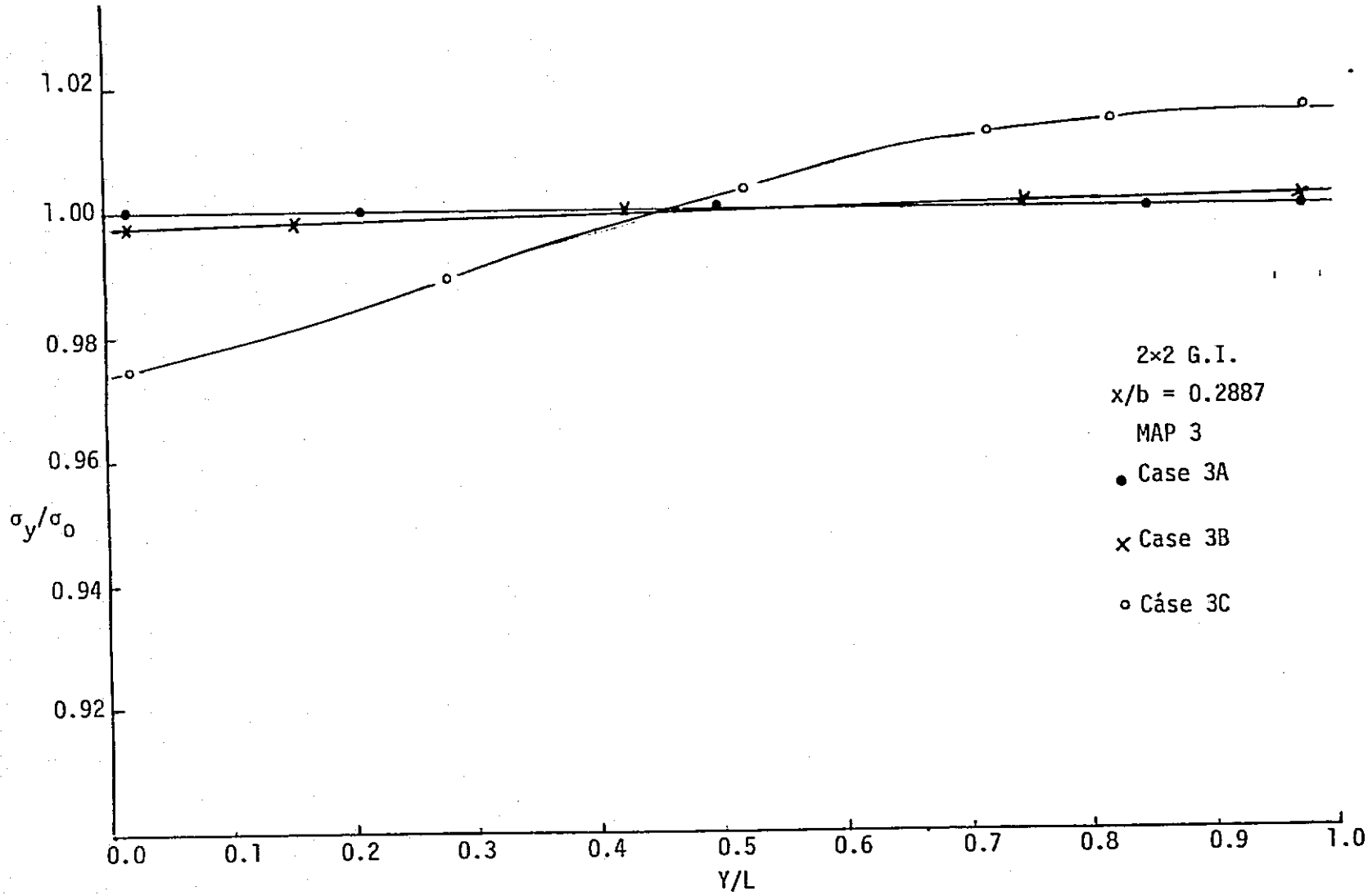

Figure 5.16

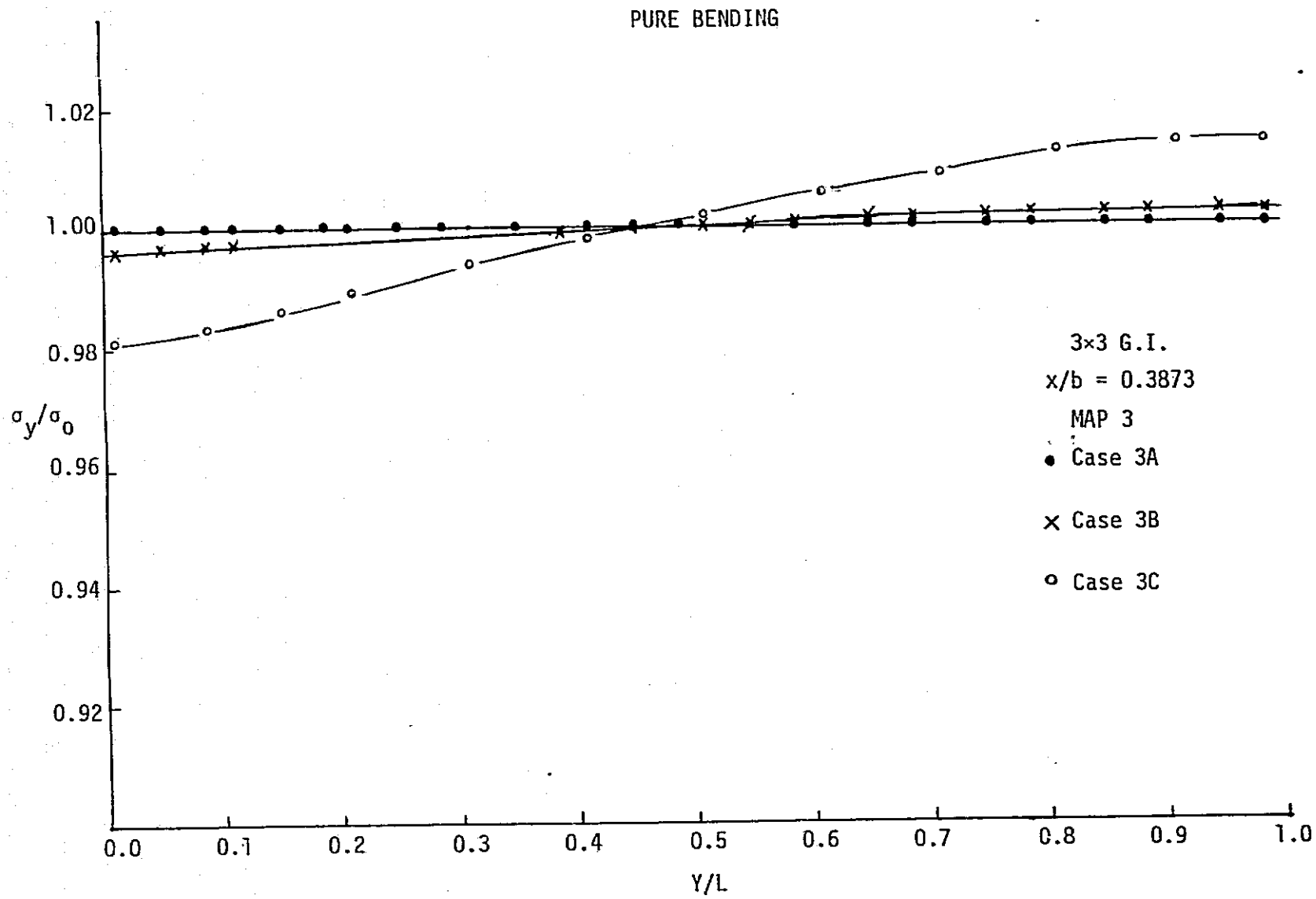
PURE BENDING
1.02
1.00
0.98
0.96
0.94
0.92
σ_y/σ_o
0.0
0.1
0.2
0.3
0.4
0.5
0.6
0.7
0.8
0.9
1.0
Y/L
3×3 G.I.
x/b = 0.3873
MAP 3
Case 3A
Case 3B
Case 3C

Figure 5.17

Case	2×2 G.I.		3×3 G.I.	
	Max. Error %	Mean Error %	Max. Error %	Mean Error %
1A	0.0010	0.0005	0.0010	0.0005
1B	0.0100	0.050	0.0010	0.0005
1C	1.3000	0.6250	0.0010	0.0005
2A	0.0010	0.0005	0.0010	0.0005
2B	0.0300	0.0150	0.0200	0.0100
2C	0.3250	0.1600	0.2500	0.1250
3A	0.0010	0.0005	0.0010	0.0005
3B	0.0250	0.0125	0.0400	0.0150
3C	0.2500	0.1050	0.1900	0.0800

Table 5.2

Similarly as is done in the pure shear problem, a study of the "assumed zero-stresses" is made for the pure bending problem. From the analytical solution, the stresses σ_x and τ_{xy} are zero. In the finite element results, these stresses are not exactly zero, but are related to the element ratio and integration scheme used, among others. Figures 5.18 to 5.23 present the variation of the shear stress τ_{xy}, along the y-axis, for the 3 maps and the two integration schemes studied. The choice of τ_{xy} instead of σ_x is arbitrary since the variation pattern of both is essentially the same. An amplification factor of 10^3 is again used. It is observed that while the error in the 2×2 G.I. scheme monotonically decreases along the y-direction, for the 3×3 G.I. scheme, the error decreases harmonically in the same direction. Table 5.3 presents a comparison of the "assumed-zero stress" error between the two

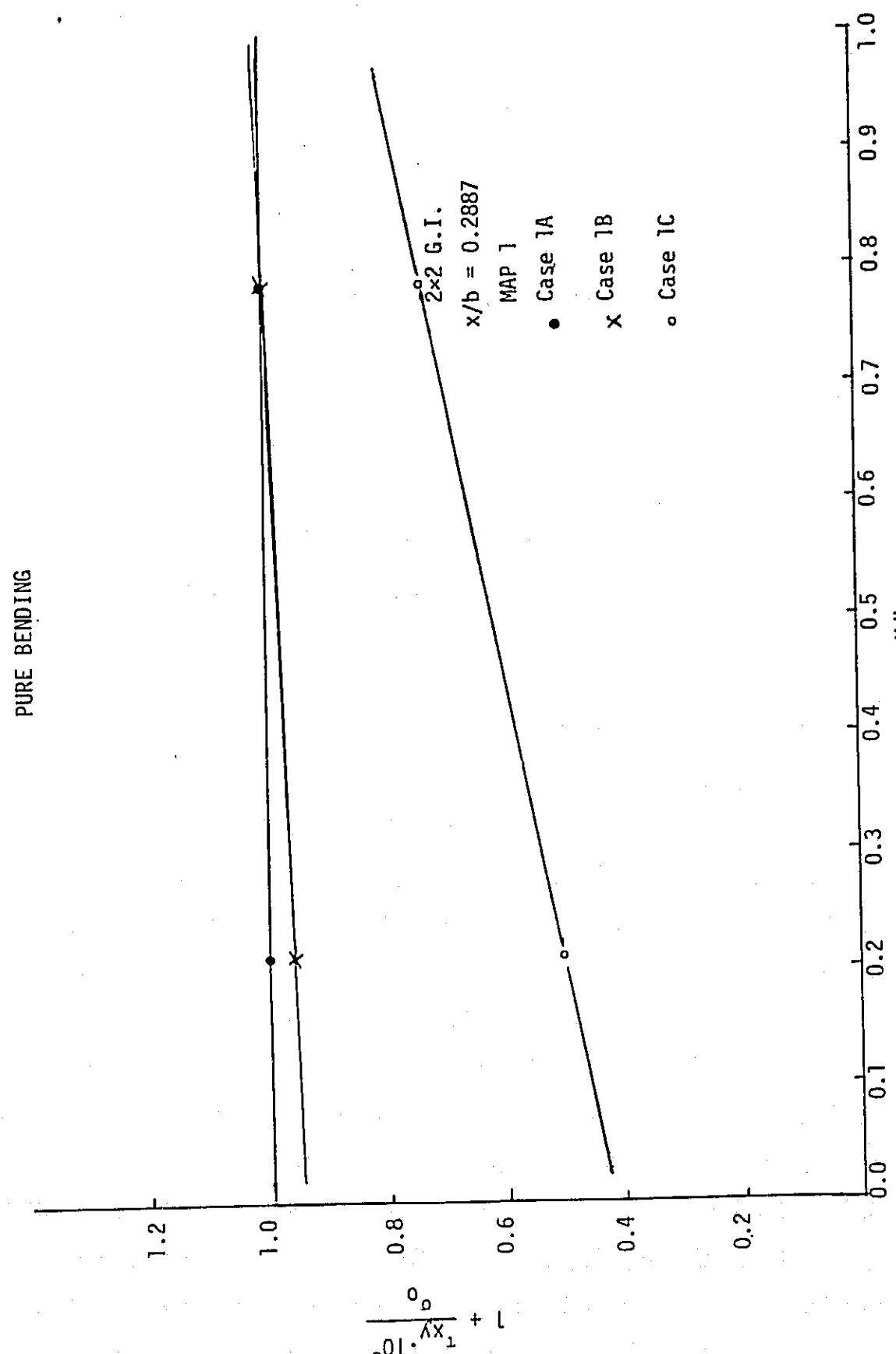
PURE BENDING
$1 + \frac{\tau_{xy} \cdot 10^3}{\sigma_o}$
1.2
1.0
0.8
0.6
0.4
0.2
0.0
0.1
0.2
0.3
0.4
0.5
0.6
0.7
0.8
0.9
1.0
Y/L
2×2 G.I.
x/b = 0.2887
MAP 1
Case 1A
Case 1B
Case 1C

Figure 5.18

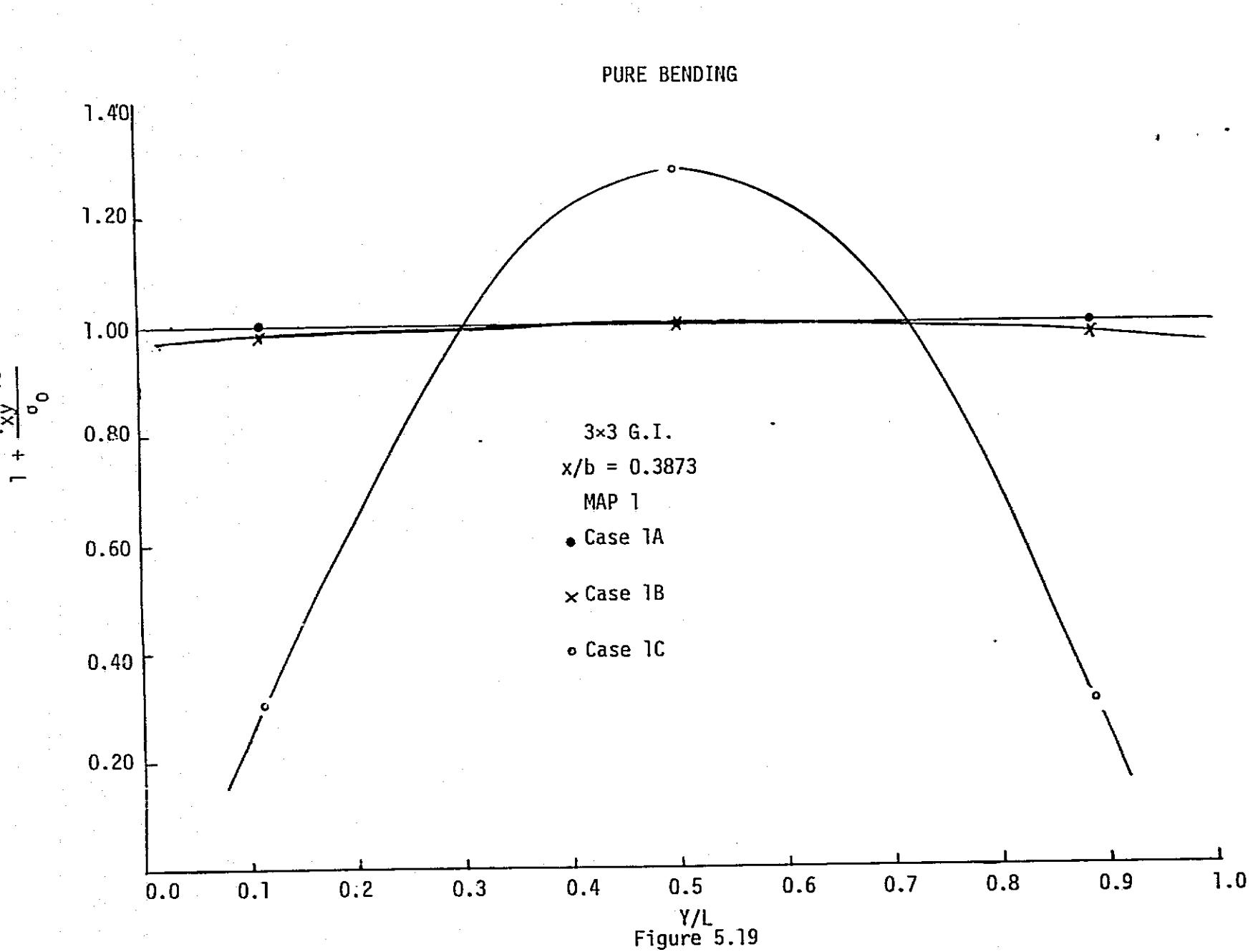
PURE BENDING
1.40
1.20
1.00
0.80
0.60
0.40
0.20
$1 + \frac{\tau_{xy} \cdot 10^3}{\sigma_o}$
3×3 G.I.
x/b = 0.3873
MAP 1
Case 1A
Case 1B
Case 1C
0.0
0.1
0.2
0.3
0.4
0.5
0.6
0.7
0.8
0.9
1.0
Y/L
Figure 5.19

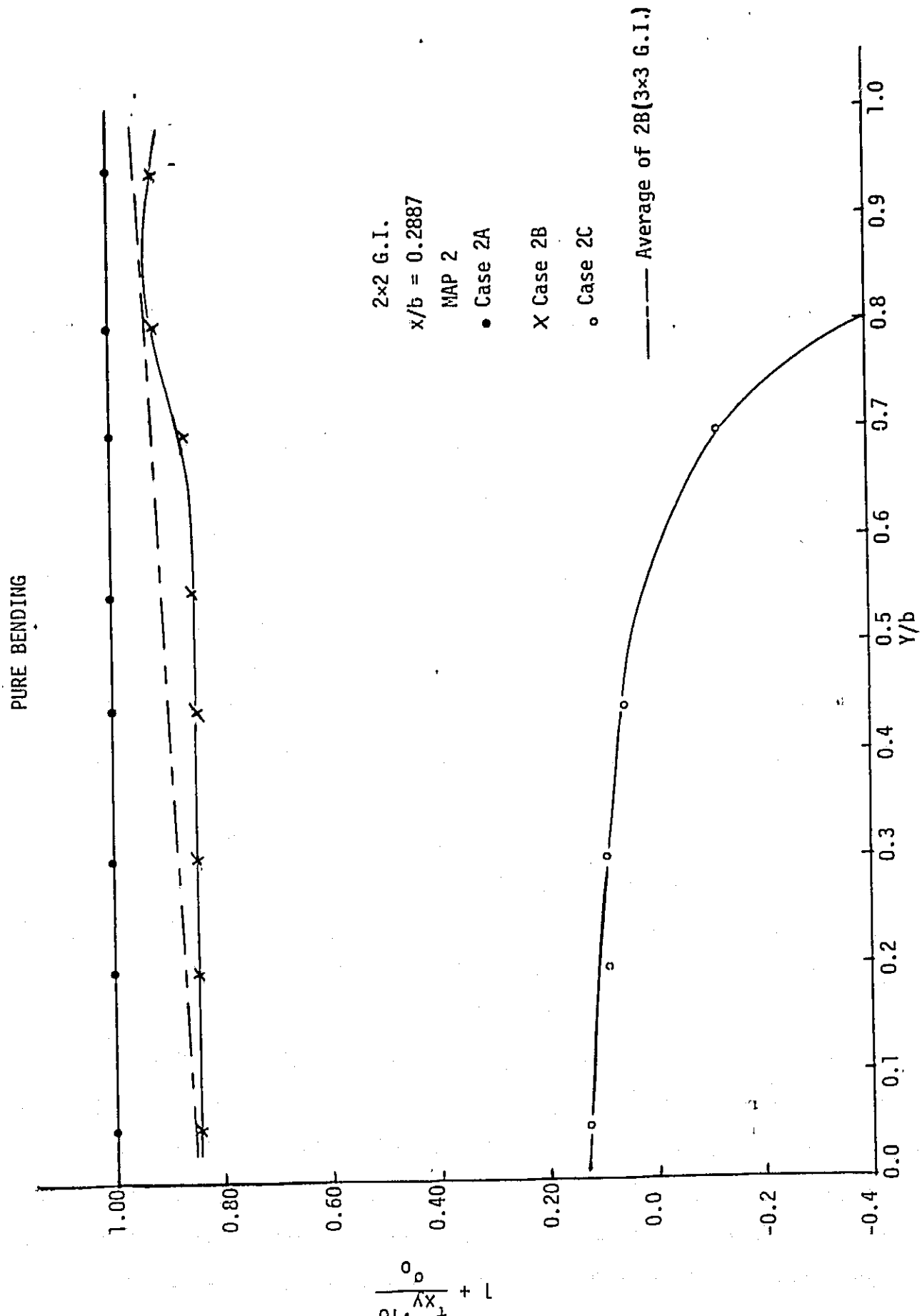
PURE BENDING
2×2 G.I.
x/b = 0.2887
MAP 2
• Case 2A
X Case 2B
o Case 2C
—— Average of 2B(3×3 G.I.)
$1 + \frac{\tau_{xy}}{\sigma_o} \cdot 10^3$
1.00
0.80
0.60
0.40
0.20
0.0
-0.2
-0.4
0.0
0.1
0.2
0.3
0.4
0.5
0.6
0.7
0.8
0.9
1.0
Y/b

Figure 5.20

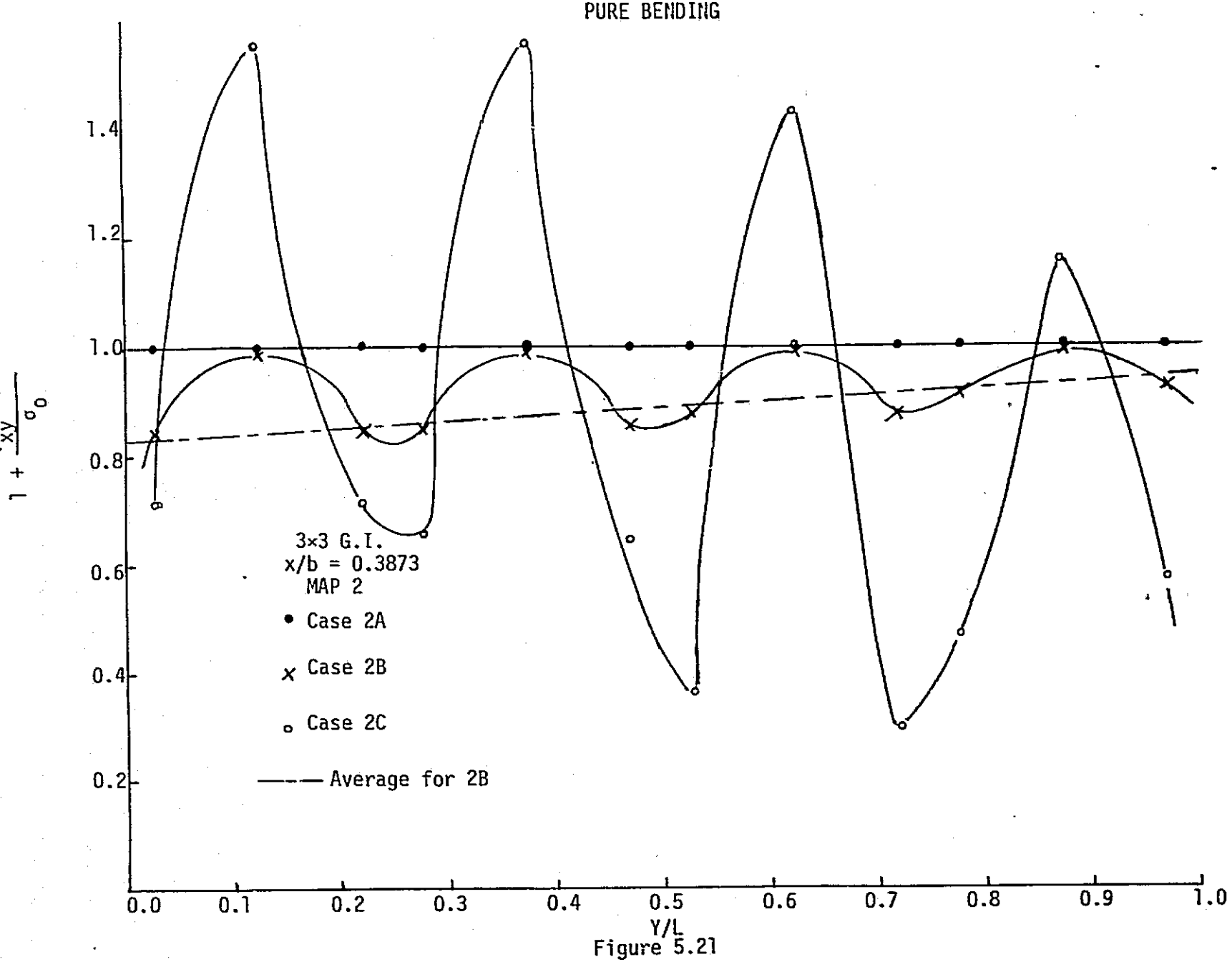
PURE BENDING
$1 + \frac{\tau_{xy} \cdot 10^3}{\sigma_o}$
1.4
1.2
1.0
0.8
0.6
0.4
0.2
3×3 G.I.
x/b = 0.3873
MAP 2
Case 2A
Case 2B
Case 2C
Average for 2B
0.0
0.1
0.2
0.3
0.4
0.5
0.6
0.7
0.8
0.9
1.0
Y/L

Figure 5.21

integration schemes studied. From the figures, it is observed that for cases A and B or any map, the difference between the two integration schemes is minimal. However, for case C, specially Maps 2 and 3, there is a considerable improvement of the 3×3 G.I. over the 2×2 G.I. scheme. It is interesting to note that the upper peaks of the curves of cases 2B, 2C, 3B, and 3C of the 3×3 G.I. scheme correspond to data provided by the same Gauss integration point of each element in the map.

Case	2×2 G.I.		3×3 G.I.	
	Max. Error %	Mean Error %	Max. Error %	Mean Error %*
1A	0.001	0.001	0.001	0.001
1B	5.000	2.750	3.000	1.500
1C	56.000	37.000	90.000	50.000
2A	0.001	0.001	0.001	0.001
2B	17.000	13.000	15.000	10.000
2C	100.000+	100.000+	70.000	45.000
3A	0.001	0.001	0.001	0.001
3B	18.000	13.000	18.000	12.500
3C	85.000	64.000	70.000	40.000

*The mean absolute error is being considered; that is

$$\% \text{ ME} = 1/n \sum_{i=1}^{n} \left| \frac{x_i}{x} \right| 100$$

Table 5.3

5.4 Execution Times

As a final comparison between the two integration schemes, the

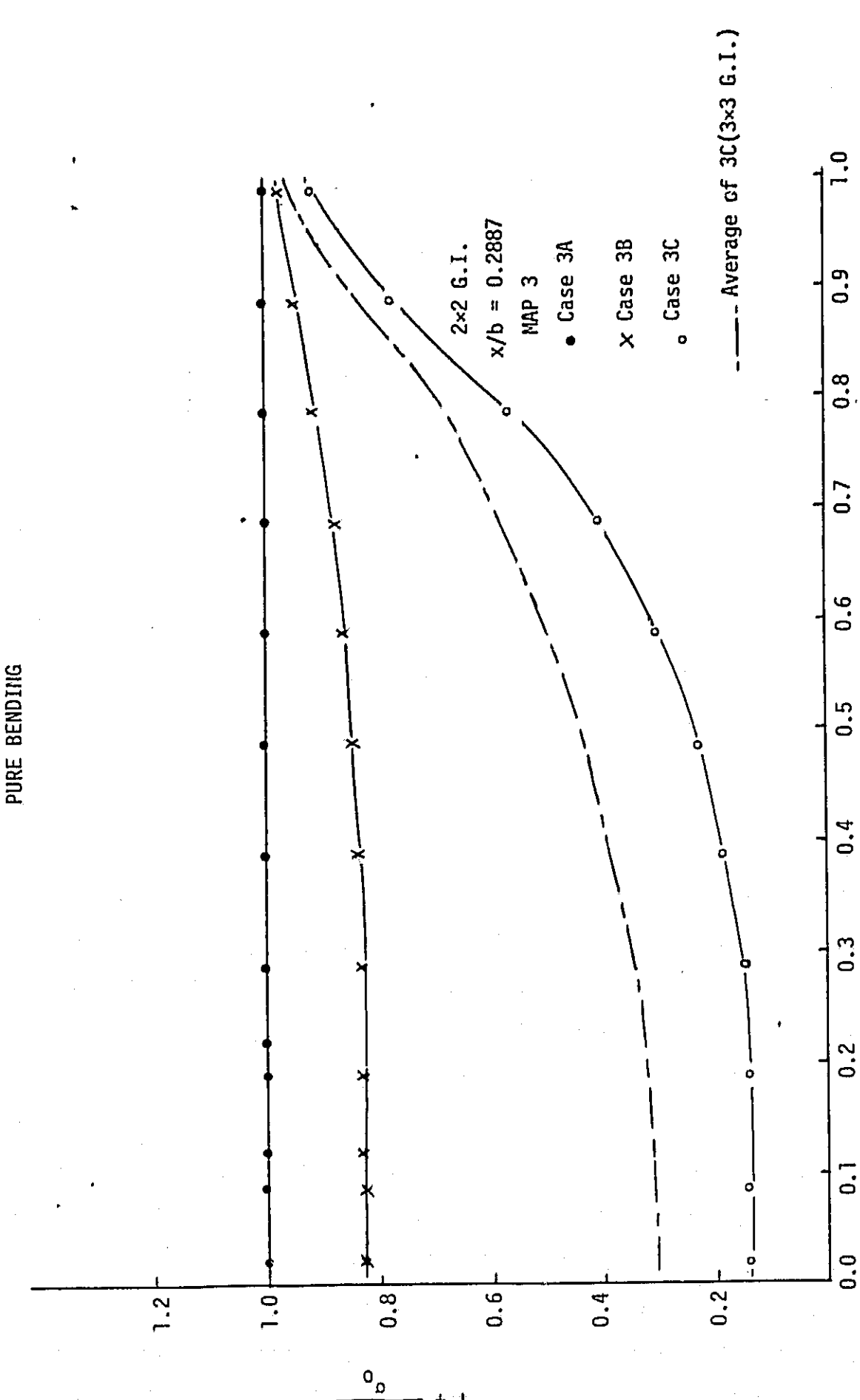
PURE BENDING
2×2 G.I.
x/b = 0.2887
MAP 3
• Case 3A
× Case 3B
∘ Case 3C
—— Average of 3C(3×3 G.I.)
$1 + \frac{\tau_{xy} \cdot 10^3}{\sigma_o}$
Y/L
0.0
0.1
0.2
0.3
0.4
0.5
0.6
0.7
0.8
0.9
1.0
0.2
0.4
0.6
0.8
1.0
1.2

Figure 5.22

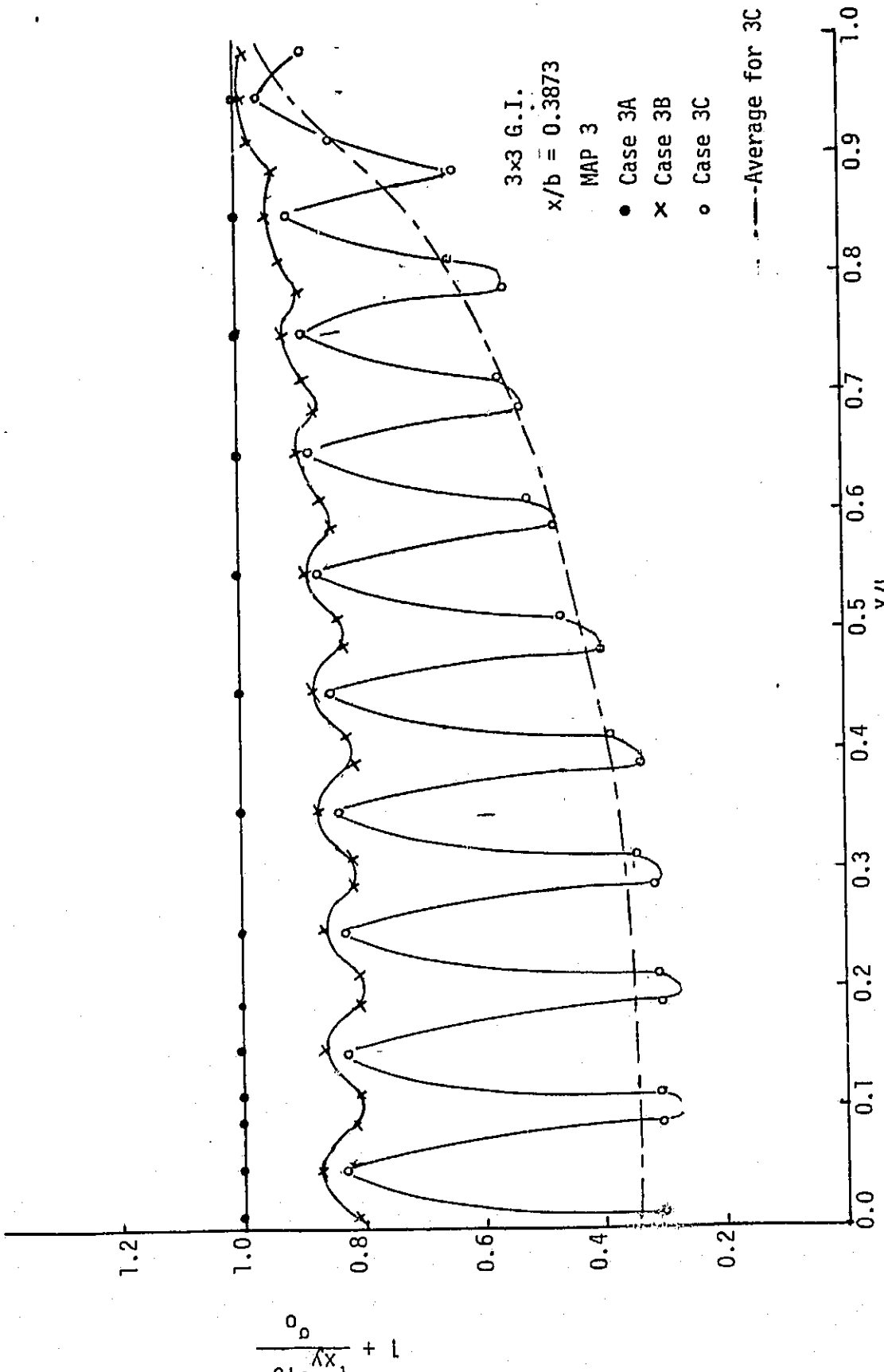
PURE BENDING
3×3 G.I.
x/b = 0.3873
MAP 3
• Case 3A
× Case 3B
o Case 3C
—·—Average for 3C
$1 + \frac{\tau_{xy} \cdot 10^3}{q_o}$
Y/L
0.0
0.1
0.2
0.3
0.4
0.5
0.6
0.7
0.8
0.9
1.0
0.2
0.4
0.6
0.8
1.0
1.2

Figure 5.23

execution times for each map obtained with the UNIVAC 1108 are studied. Since the only difference among the three cases of any map is the relative size of the elements, an average time of the three cases of each map is taken. Figures 5.24 to 5.26 present the variation of execution time with map size for the two integration schemes studied and the three problems chosen. It is observed that for Maps 1 and 2 of the uniaxial tension and pure shear problems, the execution time is almost the same, but for Map 3 the difference is considerably larger. For the pure bending problem the pattern is different. Although for Map 1 the time is the same, for Map 2, the time for the 3×3 G.I. scheme increases in 30%, but for Map 3 the difference is only of 17%. Note that the major difference in the three problems in terms of the finite element setup, is the prescription of the boundary conditions. Of course they affect the number of zero terms in the stiffness matrix and consequently the time of the routine that solves for the nodal displacements. From these time results we conclude that larger maps are necessary for better time comparisons between the two integration schemes. In [4] a time study of these integration procedures is presented for the cantilever beam problem.

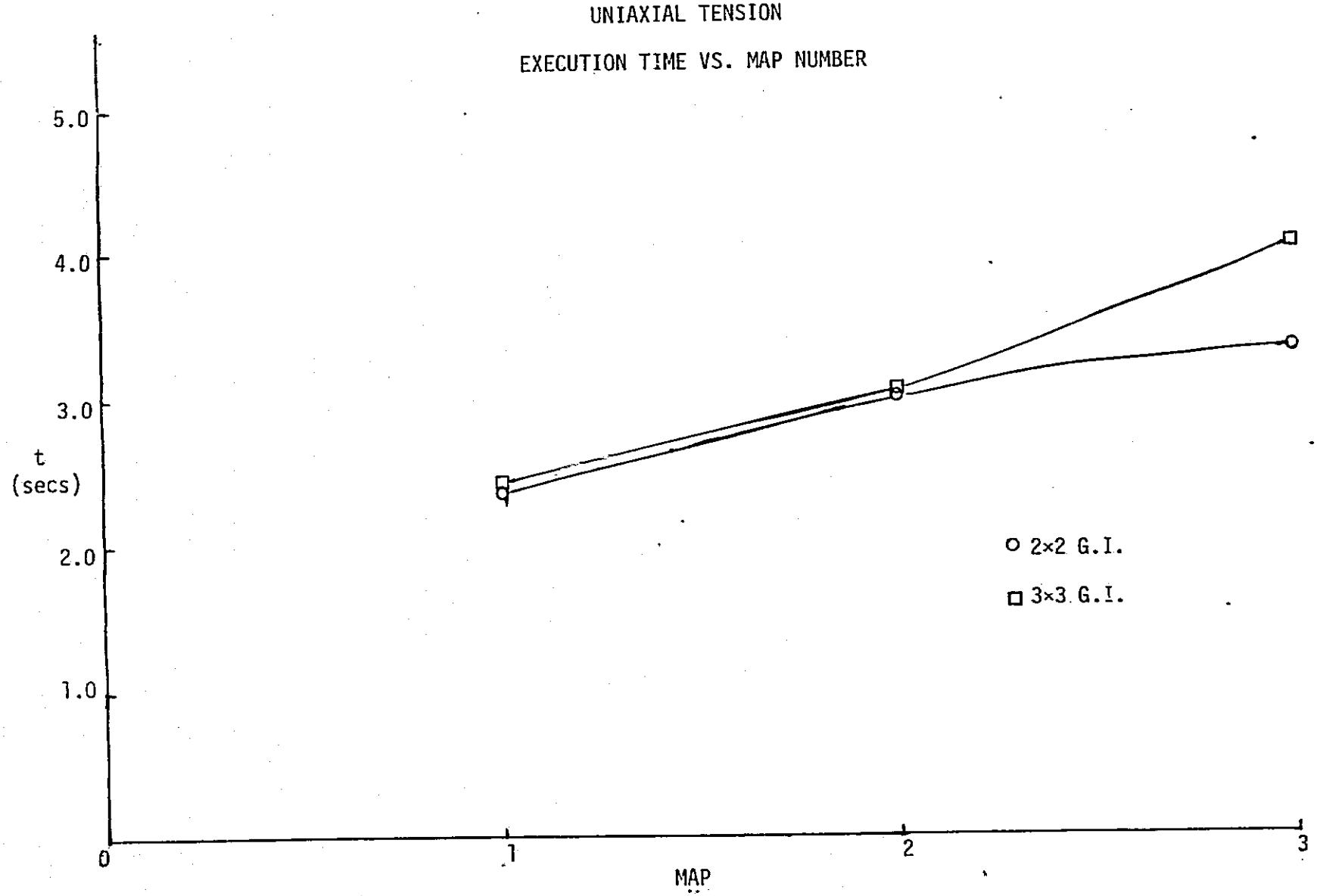
UNIAXIAL TENSION
EXECUTION TIME VS. MAP NUMBER
5.0
4.0
3.0
2.0
1.0
0
t
(secs)
1
2
3
MAP
2×2 G.I.
3×3 G.I.

Figure 5.24

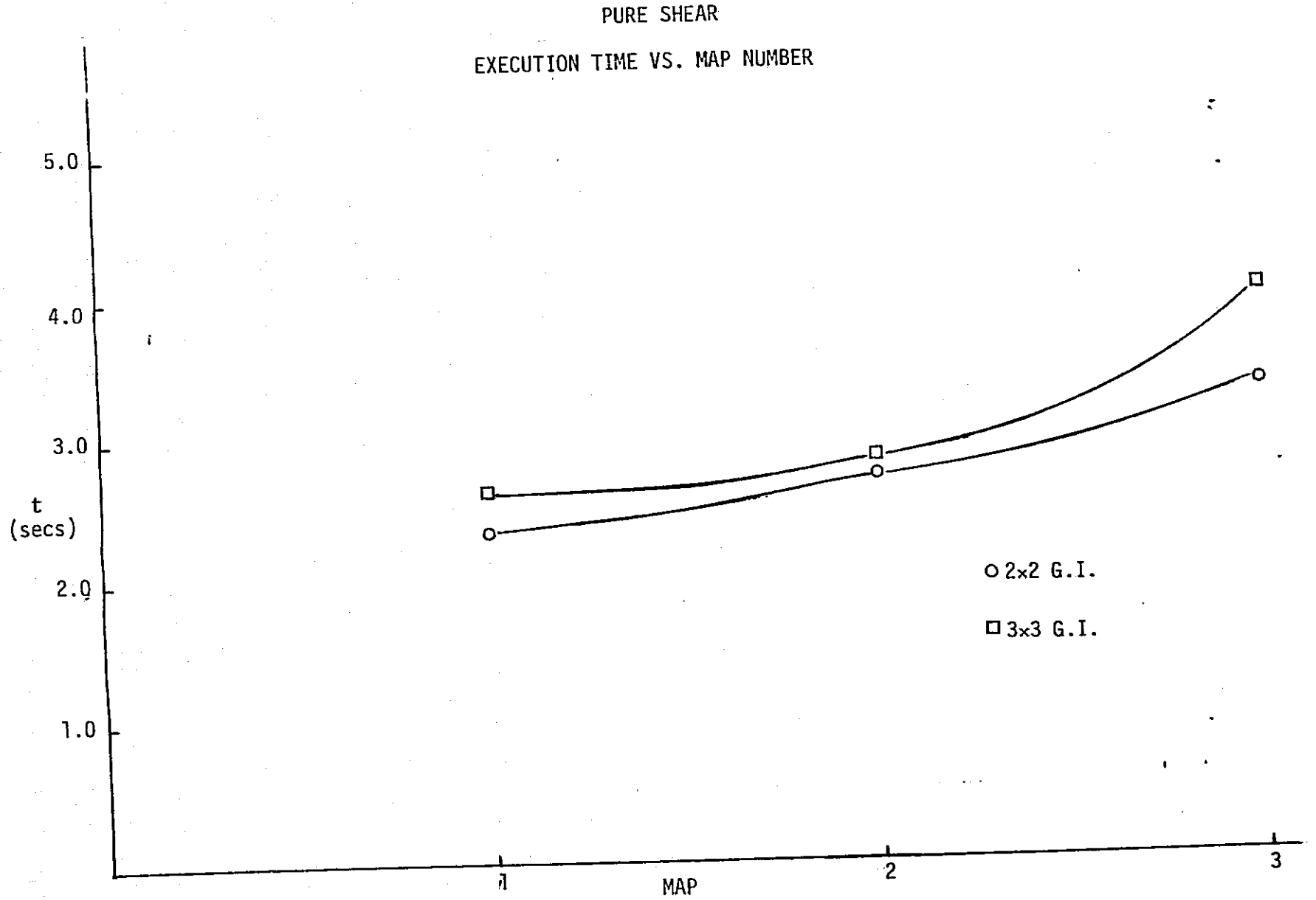
PURE SHEAR
EXECUTION TIME VS. MAP NUMBER
5.0
4.0
3.0
t
(secs)
2.0
1.0
1
MAP
2
3
2×2 G.I.
3×3 G.I.

Figure 5.25

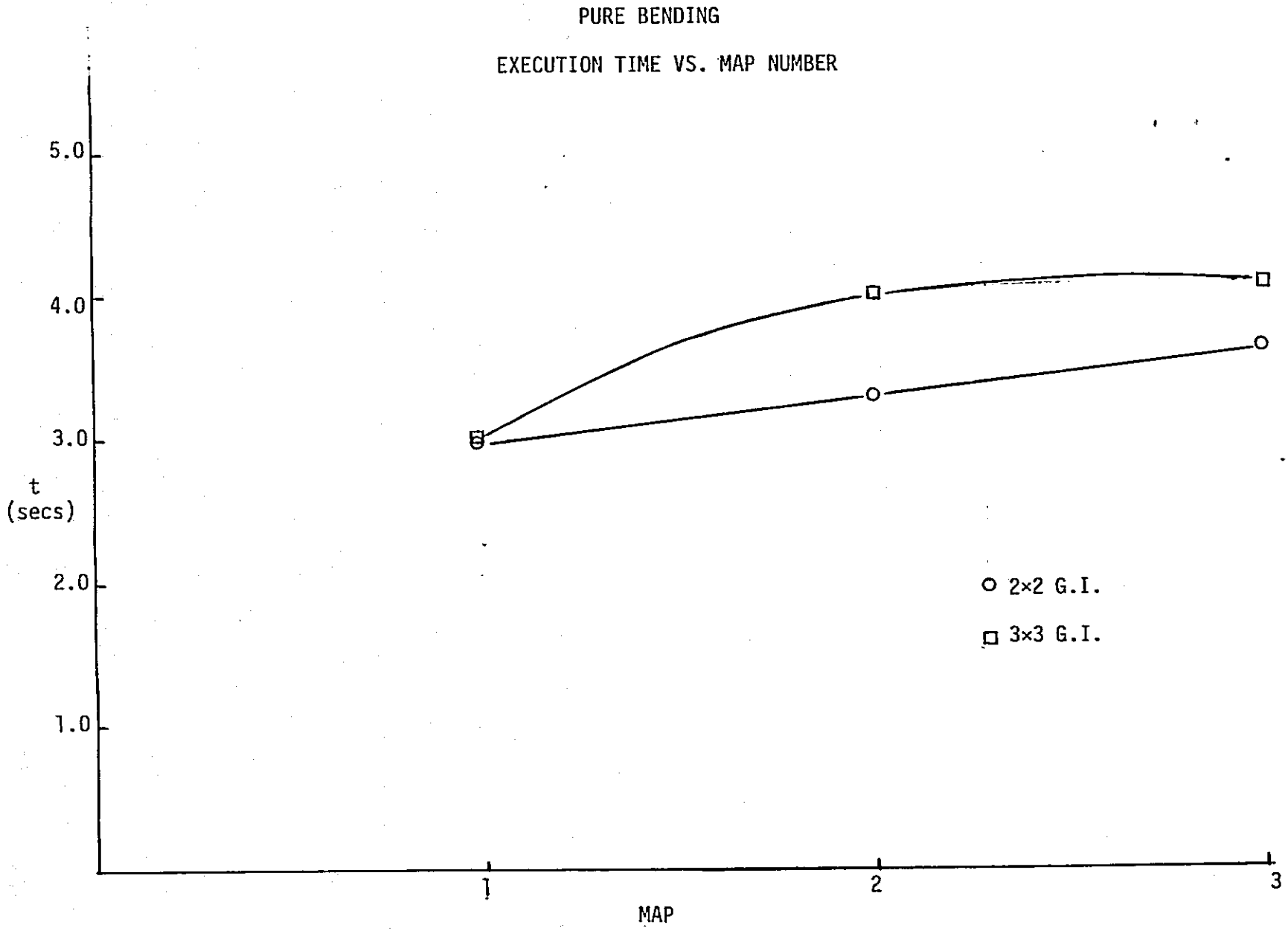
PURE BENDING
EXECUTION TIME VS. MAP NUMBER
5.0
4.0
3.0
2.0
1.0
t
(secs)
2×2 G.I.
3×3 G.I.
1
2
3
MAP

Figure 5.26

6. CONCLUSIONS AND RECOMMENDATIONS

It is concluded in the report that the eight-node isoparametric quadrilateral presents many of the features of the high-order elements with the advantage that there is no need to resort to expensive and complex integration schemes.

It is shown that although the element contains in its formulation the exact solution for tension, shear and pure bending problems, the actual results are highly dependent upon the slenderness of the element in a given map, as well as the numerical integration scheme used. As more terms of the displacement functions of the element enter in the solution of a problem (linear terms for tension; quadratic terms for shear; cubic terms for pure bending, etc.) these effects must be carefully considered in the accuracy of the solution.

The results studied show that although the 2×2 G.I. scheme provides adequate solutions, the penalty of using 3×3 G.I. instead is not high in terms of storage and computation time, but the benefit is substantially higher. This is particularly true in problems containing more complex geometry and loading, where the displacement solution is not contained in the element formulation. The same is valid for elasto-plastic problems where the location and size of the yielding zone is important, and where the construction of the stiffness matrix of an element that has yielded requires a higher-order integration procedure.

In the transition to solve plasticity problems, apart from reserving some storage area for quantities such as accumulated forces and displace-

ments, plastic strain energy, plastic stresses and strains, the major change lies on the constitutive matrix, [D]. This matrix is direct function of the state of loading, once yielding has occurred. This analysis is based on the theory of elasto-plastic flow described in detail in [8,9]. At any particular Gauss point where yielding has taken place the stress-strain matrix [D] must be updated at each loading step according to the current level of stress at that point. Hence, essentially only the assembly of the element stiffness matrix gets changed since a different constitutive matrix might be needed for each Gauss point.

Looking toward a general stress program for large computers, which would apply to realistic nonlinear material behavior of cracked structures, it is considered convenient to make the program capable to accept other element configurations, such as special crack-tip elements, or even other isoparametric elements. Furthermore, it should be possible to think in a quadrilateral having a cubic response along one side which contains four nodes, linear response along other side with only two corner nodes, and quadratic along the other two. The coupling of a higher order element to lower elements may be accomplished by constraining the coupling surface of the higher order element to displace in accordance to the lower order element.

Finally, a desirable feature of any large computer program is an internal map generation algorithm. Because of the midside node in the isoparametric quadrilateral, the data preparation is considerably reduced by writing into the program an algorithm which interpolates the positions of midside node coordinates if the sides are straight. Only when the

particular side is required to follow a curved boundary is it necessary to specify all intermediate nodes. However, algorithms for circumferential element profiles are easy to implement.

ACKNOWLEDGMENTS

The author is grateful to Professor J. L. Swedlow and Dr. J. R. Osias for their continuous advice and critical review of this paper. The assistance of Ms. Stella DeVito in the preparation of the manuscript is greatly appreciated.

REFERENCES

[1] Zienkiewicz, O. C., The Finite Element Method in Engineering Science, McGraw-Hill, 1973.

[2] Zienkiewicz, O. C., and C. J. Parekh, "Transient Field Problems: Two Dimensional and Three Dimensional Analysis by Isoparametric Finite Elements," IJNME, Vol. 2, 1970, pp. 61-71.

[3] Ergatoudis, I., B. M. Irons, and O. C. Zienkiewicz, "Curved, Isoparametric Quadrilateral Elements for Finite Element Analysis," International Journal of Solids Structures, Vol. 4, 1968, pp. 31-42.

[4] Marino, C., "A Solution to the Cantilever Beam Problem using the Eight-Node Isoparametric Quadrilateral," Report SM-75-3, Department of Mechanical Engineering, Carnegie-Mellon University, 1975.

[5] Gupta, A. K., "Elasto-Plastic Analysis of Three-Dimensional Structures using the Isoparametric Element," Nuclear Engineering and Design, Vol. 22, 1972, pp. 305-317.

[6] Irons, B. M., "Engineering Applications of Numerical Integration in Stiffness Methods," AIAA Journal, Vol. 4, 1966, pp. 2035-2037.

[7] Carnahan, B., H. A. Luther, and J. O. Wilkes, Applied Numerical Methods, John Wiley & Sons, Inc., New York, 1969.

[8] Swedlow, J. L., "A Procedure for Solving Problems of Elasto-Plastic Flow," Computer Structures, Vol. 3, 1973, pp. 879-898.

[9] Swedlow, J. L., "Character of the Equations of Elasto-Plastic Flow in Three Independent Variables," International Journal of Non-Linear Mechanics, Vol. 3, 1968, pp. 325-336; Vol. 4, 1969, p. 77.

APPENDIX A

The partial derivatives of the displacement functions for the 8-Node isoparametric quadrilateral are the following:

(a) Corner Nodes $i = 1,3,5,7$

In ξ:

$$\frac{\partial N_i}{\partial \xi} = 1/4\ \xi_i(1 + \eta\eta_i)(\xi\xi_i + \eta\eta_i - 1) + 1/4(1 + \xi\xi_i)(1 + \eta\eta_i)\xi_i$$

Or, $$\frac{\partial N_i}{\partial \xi} = 1/4\ \xi_i(1 + \eta\eta_i)(2\xi\xi_i + \eta\eta_i) \qquad (A1)$$

In η:

$$\frac{\partial N_i}{\partial \eta} = 1/4\ \eta_i(1 + \xi\xi_i)(\xi\xi_i + \eta\eta_i - 1) + 1/4(1 + \xi\xi_i)(1 + \eta\eta_i)\eta_i$$

Or, $$\frac{\partial N_i}{\partial \eta} = 1/4\ \eta_i(1 + \xi\xi_i)(\xi\xi_i + 2\eta\eta_i) \qquad (A2)$$

(b) Midside Node, $\xi_i = 0$; $i = 2,6$

In ξ:

$$\frac{\partial N_i}{\partial \xi} = -\ \xi(1 + \eta\eta_i) \qquad (A3)$$

In η:

$$\frac{\partial N_i}{\partial \eta} = 1/2\ \eta_i(1 - \xi^2) \qquad (A4)$$

(c) Midside Nodes, $\eta_i = 0$; $i = 4,8$

In ξ:

$$\frac{\partial N_i}{\partial \xi} = 1/2\ \xi_i(1 - \eta^2) \qquad (A5)$$

In η:

$$\frac{\partial N_i}{\partial \eta} = -\eta(1 + \xi\xi_i) \qquad (A6)$$